Available online at www.sciencedirect.com

SCIENCE DIRECT®

Journal of Volcanology and Geothermal Research 137 (2004) 109–134

Journal of volcanology and geothermal research

www.elsevier.com/locate/jvolgeores

Acoustic measurements of the 1999 basaltic eruption of Shishaldin volcano, Alaska 1. Origin of Strombolian activity

S. Vergniolle[a,*], M. Boichu[a], J. Caplan-Auerbach[b,1]

[a] *Laboratoire de Dynamique des Systèmes Géologiques, Institut de Physique du Globe de Paris, 4 Place Jussieu, Paris Cedex 05 75252, France*
[b] *Alaska Volcano Observatory, Geophysical Institute, University of Alaska, Fairbanks, USA*

Abstract

The 1999 basaltic eruption of Shishaldin volcano (Alaska, USA) displayed both classical Strombolian activity and an explosive Subplinian plume. Strombolian activity at Shishaldin occurred in two major phases following the Subplinian activity. In this paper, we use acoustic measurements to interpret the Strombolian activity.

Acoustic measurements of the two Strombolian phases show a series of explosions that are modeled by the vibration of a large overpressurised cylindrical bubble at the top of the magma column. Results show that the bubble does not burst at its maximum radius, as expected if the liquid film is stretched beyond its elasticity. But bursting occurs after one cycle of vibration, as a consequence of an instability of the air–magma interface close to the bubble minimum radius. During each Strombolian period, estimates of bubble length and overpressure are calculated. Using an alternate method based on acoustic power, we estimate gas velocity to be 30–60 m/s, in very good agreement with synthetic waveforms.

Although there is some variation within these parameters, bubble length and overpressure for the first Strombolian phase are found to be $\approx 82 \pm 11$ m and 0.083 MPa. For the second Strombolian phase, bubble length and overpressure are estimated at 24 ± 12 m and 0.15 MPa for the first 17 h after which bubble overpressure shows a constant increase, reaching a peak of 1.4 MPa, just prior to the end of the second Strombolian phase. This peak suggests that, at the time, the magma in the conduit may contain a relatively large concentration of small bubbles. Maximum total gas volume and gas fluxes at the surface are estimated to be 3.3×10^7 and 2.9×10^3 m^3/s for the first phase and 1.0×10^8 and 2.2×10^3 m^3/s for the second phase. This gives a mass flux of 1.2×10^3 and 8.7×10^2 kg/s, respectively, for the first and the second Strombolian phases.

Keywords: Shishaldin; eruption dynamics; acoustics; Strombolian activity; bubble

1. Introduction

The most common explosive eruptive behaviours observed for basaltic volcanoes are periodic fire fountains (Hawaiian activity) or regular explosions (Strombolian activity). Both eruptive types are driven by large gas pockets, with a size on the order of the conduit radius for Strombolian explosions or much longer for Hawaiian fire fountains (Vergniolle and Jaupart, 1986). One characteristic feature is an alternating between a phase rich in gas and a phase relatively poor in gas (Jaupart and Vergniolle, 1988,

* Corresponding author.
[1] Now at the Alaska Volcano Observatory, U.S. Geological Survey, Anchorage, AK, USA.

0377-0273/$ - see front matter © 2004 Elsevier B.V. All rights reserved.
doi:10.1016/j.jvolgeores.2004.05.003

1989; Vergniolle and Jaupart, 1990). The formation of the gas rich phase, i.e. a fire fountain for Hawaiian volcanoes and regular explosions for Strombolian volcanoes, is a consequence of small gas bubbles rising in the reservoir. These bubbles rise and accumulate at the top, where a foam layer builds. When the foam reaches a critical thickness, it collapses either totally for very fluid lava (Hawaiian case) or partially for more viscous lava (Strombolian case). The formation of a large gas pocket in the conduit leads to a fire fountain or a Strombolian explosion (Jaupart and Vergniolle, 1988, 1989; Vergniolle and Jaupart, 1990).

Understanding eruption behaviour requires a clear understanding of flow parameters, such as pressure and velocity, variables which are necessary for modelling the flow of magma and gas from depth to the surface. Because it is obviously impossible to measure these parameters directly, our best hope is to constrain these values at the surface. For a long time, however, the only estimates of physical parameters during surface activity came from visual observations, such as the height reached by ejecta (Blackburn et al., 1976; Wilson, 1980; Wilson and Head, 1981) or from studies of photoballistics (Chouet et al., 1974; McGetchin et al., 1974; Ripepe et al., 1993). For example, observations have been made of gas bubbles breaking at the surface of volcanoes such as Heimaey (Iceland) and Stromboli (Italy) (Self et al., 1974; Blackburn et al., 1976; Wilson, 1980). Using estimates of gas velocity, overpressure during Strombolian activity was estimated at ≈ 0.025 MPa for Heimaey and at ≈ 600 Pa for Stromboli (Blackburn et al., 1976). Such measurements yield typical Strombolian gas velocities of less than 100 m/s (Chouet et al., 1974; McGetchin et al., 1974; Blackburn et al., 1976), while gas velocities estimates for Hawaiian fire fountains reach 100 or 200 m/s (Wilson, 1980; Wilson and Head, 1981; Vergniolle and Jaupart, 1990). Direct geophysical measurements of gas and ejecta velocities, during Strombolian activity, have confirmed these values either by the use of a sodar (Weill et al., 1992) or by a radar (Hort and Seyfried, 1998; Dubosclard et al., 1999, in press) pointed towards the active vent.

Until recently, measurements of acoustic waves produced by an erupting volcano have been relatively sparse. This is primarily due to the fact that for many years low cost instruments could only measure audible frequencies (above 20 Hz) (Richards, 1963; Woulff and McGetchin, 1976) and volcanic sound waves are primarily infrasonic. Recent technologies have allowed these frequencies to be recorded and show that they can be used to estimate source characteristics (Vergniolle and Brandeis, 1994, 1996; Vergniolle et al., 1996; Hagerty et al., 2000). On volcanoes, such as Stromboli (Buckingham and Garcès, 1996) or Pavlof (Garcès and McNutt, 1997), the propagation of acoustic pressure in the shallow magma and its transport towards the atmosphere has been calculated.

There are three main models that have been developed for volcanic acoustic signals. The first class of acoustic models associates the frequency and amplitude of acoustic signals with resonant modes of the shallow volcanic conduit (Buckingham and Garcès, 1996; Garcès et al., 2000; Hagerty et al., 2000). While useful for some volcanoes, a resonating conduit model, when applied to Stromboli, leads to extremely high values of viscosity (9×10^5 Pa s) and source overpressure (1×10^3 MPa) at shallow depth (Buckingham and Garcès, 1996). At Arenal volcano (Costa Rica), an explosive source, buried at 12 m below the surface and with an overpressure of 3.4 MPa produces an excellent, although non-unique fit to the observed acoustic waveforms (Hagerty et al., 2000).

The second class of acoustic models suggest that sound is produced when the volcano is suddenly uncorked after reaching a pressure threshold. Uhira and Takeo (1994) suggest that the overpressure in the source is at least 0.3 MPa at Sakurajima volcano (Japan). For Johnson et al. (1998) and Johnson and Lees (2000), Vulcanian explosions, corresponding to the disruption of a plug at the top of the magma column, are characteristic of a magma with intermediate viscosity, such as those seen at Karymsky (Kamchatka, Russia), Sangay (Ecuador) and Arenal volcanoes (Costa Rica).

In contrast, volcanoes with fluid lava, such as Stromboli, Kilauea (Hawaii), Villarica (Chile), Erebus (Antartica) keep an open vent through which large gas bubbles can escape and burst (Sparks et al., 1997). In this type of activity, sound is produced by the strong vibration of a large cylindrical bubble prior to its bursting at the top of the magma column (Vergniolle and Brandeis, 1994, 1996; Vergniolle et al., 1996). At

Stromboli, acoustic data have been used to determine parameters such as bubble radius (≈ 1 m), length (between 1 and 20 m) and bubble overpressure (≈ 0.10 MPa) (Vergniolle and Brandeis, 1996). Because a bubble approaching an interface can develop kinematic waves whose frequency depends on viscosity, the bubble at Stromboli is also heard rising in the uppermost few tens of meters of the conduit before breaking (Vergniolle et al., 1996).

In this paper, we describe the 1999 basaltic eruption of Shishaldin volcano (Alaska, USA) during two Strombolian phases and quantify the source of acoustic signals recorded at a distance of 6.5 km from the vent. Acoustic data show a series of explosions, the waveforms of which are surprisingly similar to those recorded at Stromboli volcano. Therefore, the sound wave produced by each explosion is modelled, as for Stromboli, by the vibration induced by residual overpressure inside the bubble, prior to bursting at the magma surface. The best fit between the model and the explosion waveforms allows us to estimate bubble radius, length and overpressure during the course of the eruption. We show that acoustic sensors, which can give very good estimates on the gas velocity from acoustic power, are both reliable and easy to implement for volcanic monitoring.

2. Setting and materials

Shishaldin volcano is located on Unimak Island, the first island in the Aleutian arc (Fig. 1). Its historical eruptions have been primarily Strombolian in nature, producing steam and moderate height ash plumes of basalt and basaltic andesite. Rare instances of andesite or dacite eruptions have also been noted (Fournelle, 1988). Large volume tephra layers, whose origin might be Subplinian, are seen with an occurrence of 11 in the past 9 ka, whereas classical basaltic eruptions occur with an intermittency of ≈ 20 eruptions/century (Beget et al., 1998; Nye et al., 2002).

In 1997, a six-station seismic network was installed near Shishaldin by the Alaska Volcano Observatory (AVO) (Fig. 1). Five of the stations are short period

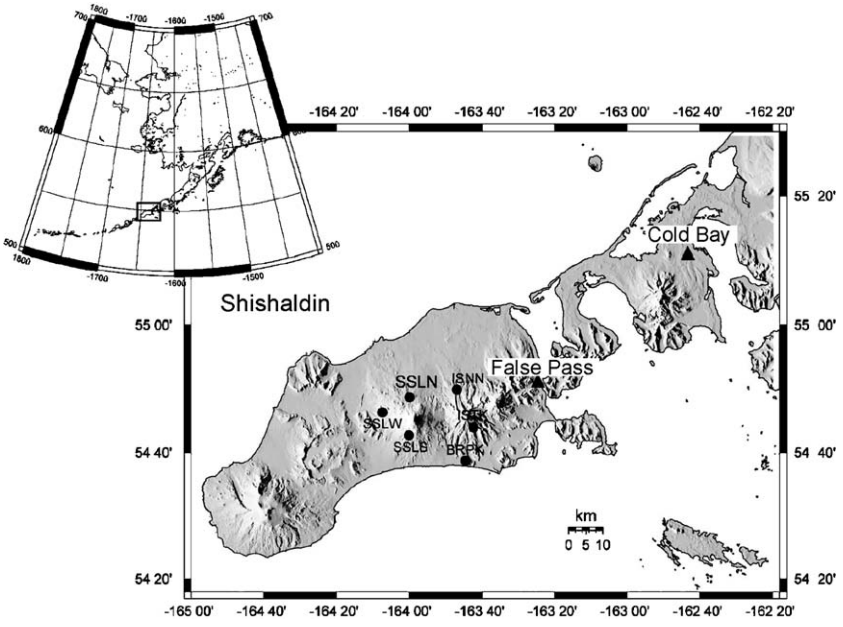

Fig. 1. Location of Shishaldin volcano and Unimak Island, Alaska. Black circles represent the locations of the short-period network operated by the Alaska Volcano Observatory. The pressure sensor used to collect the acoustic data in this study is co-located with station SSLN on the north flank of Shishaldin. The two nearest population centers, False Pass and Cold Bay, are marked with triangles.

Mark Products L-4C instruments with natural period of 1 s. Station SSLS is a three component Mark Products L-22 instrument with 0.5-s natural period. A Setra 239 pressure sensor, with a theoretical sensitivity of 0.36 mV/Pa, was co-located with station SSLN on the volcano's north flank and has recorded signals without saturation.

In 1997, at the time that the pressure sensor was deployed at Shishaldin, no calibration facility existed at the University of Alaska Fairbanks (UAF). Consequently, the instrument was nominally calibrated by comparing its output to that of a calibrated Bruel and Kjaer microphone (Garcès et al., 2001, pers. com.). At this time the sensitivity was found to be ≈ 0.2 mV/Pa a value used in an initial study of the pressure sensor data (Caplan-Auerbach and McNutt, 2003). Unfortunately, the reference microphone was only calibrated at high frequencies (≥ 1 Hz), with uncalibrated sources used at lower frequencies. Attempts to calibrate the instrument when it was retrieved in 2003 were unsuccessful due to an apparent fault within the pressure sensor. The instrument was subsequently returned to Setra for calibration where it was confirmed to be operating at its theoretical sensitivity. The theoretical transfer function for the pressure sensor, telemetry system and digitizer is flat for frequencies ≤ 4 Hz (Fig. 2).

In the field, the pressure sensor was installed in a plastic box and mounted on the wall of the fiberglass hut in which batteries and electronics were also housed. The reference port was covered with a prophylactic membrane (M. Garcès, highly pers. com., 2003) so that the port was protected from dirt or snow. A pipe from the active port (diameter of ≈ 1 cm) ran from the casing through the leeward wall of the hut, where it was positioned ≈ 15 cm above the hut flange, directed toward the ground to further minimise the effects of wind. The effect of the housing in instrument response is unknown. However, we note that while the specific values recorded by the pressure sensor carry a small degree of uncertainty, this does not affect our interpretation of the sequence of events in the 1999 eruption. Data from all instruments are telemetered to Cold Bay or King Cove and then to AVO over analog telephone lines. Finally the data are low-pass filtered with a corner frequency of 20 Hz and sampled at 100 Hz with 12-bit resolution. Although the anti-aliasing filter diminishes signal amplitudes at high frequencies, this effect is minimal at frequencies ≤ 4 Hz, the frequency band in which most of the data discussed here are found.

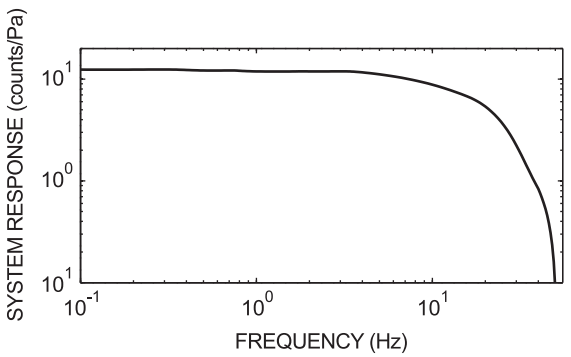

Fig. 2. Theoretical transfer function for the pressure sensor, telemetry system and digitizer. Note that the response is flat for all frequencies below ≈ 4 Hz.

The greatest source of uncertainty with respect to signals recorded by the pressure sensor is in discriminating between volcanic signals and signals produced by other sources such as wind. The nearest weather station to Shishaldin is stationed in Cold Bay (Fig. 1), over 90 km from the volcano. Moreover, it is likely that a volcano the size of Shishaldin has a significant effect on the local wind field. Consequently, wind conditions at the pressure sensor site were unknown at the time of the eruption. However, an unidentified low frequency (0–3 Hz) signal bearing little to no resemblance to the waveforms recorded at the time of the eruption was commonly recorded on the pressure sensor. This signal was observed both before and after the eruption, suggesting that its source was non-volcanic, and possibly due to the wind. However, we were careful to consider wind as a potential source for each of the signals recorded during the eruption as well.

3. Eruption activity

Although tremor and satellite thermal anomalies indicated unrest at Shishaldin as early as January 1999, the first confirmation of eruptive activity was not made until April 18, 1999. At this time, AVO researchers performed an overflight of the volcano. Although a thick cloud obscured Shishaldin's summit, imagery acquired with a Forward Looking Infrared

Radiometer (FLIR) shows the first confirmed spattering activity, with ejection of lava ≈ several tens of meters above the crater wall (Nye et al., 2002). After 30 h of apparent quiet, a series of tiny bursts were detected by the pressure sensor. This phase, referred to as the "hum" lasted 13 h and was followed by a dramatic increase in seismic tremor accompanied by an ash plume to heights above 16 km (Caplan-Auerbach and McNutt, 2003). This Subplinian eruption is believed to be responsible for the majority of ejecta produced by Shishaldin in 1999 (Stelling et al., 2002). The Subplinian phase was immediately followed by the first major Strombolian phase, lasting 3.5 h. Explosions recorded during this phase have mean frequencies near 0.7–0.8 Hz and mean amplitudes of 1–2 Pa at 6.5 km from the vent. Two small bursts of Strombolian activity occurred 2 and 7 h after the first major Strombolian phase. Because these correspond to bubbles just at the limit of detection and they occurred for only a short time (<1 h), they will be ignored here. After 60 h of quasi-quiescence, the second Strombolian phase began and lasted almost 24 h (April 22–23, 1999). These events have power spectral peaks near 1.1–1.5 Hz. For the first 17 h of this phase, explosions have amplitudes of 0.5–4 Pa. During the final 4 h of this phase, acoustic pressure increased dramatically, with peak amplitudes exceeding 30 Pa (Caplan-Auerbach and McNutt, 2003). After this Strombolian phase, the eruption decreased in intensity. However there were several ash plumes in April (23rd, 26th) and May (13th, 25th, 26th) before the eruption definitively ended.

Most of the following interpretation of the eruption is based on data from the pressure sensor, co-located with station SSLN at 6.5 km from the vent (Fig. 1). The first acoustic signals that can be definitively associated with the eruption were recorded after the observed spattering activity on April 18, 1999. All of the nearest seismic stations, including the station co-located with the pressure sensor (SSLN; Fig. 1), were saturated by strong tremor during most of the eruption, making it difficult to directly compare seismic and acoustic signals (Caplan-Auerbach and McNutt, 2003). The other seismometers provide qualitative information on the frequency spectra inside the volcanic edifice. All this information is combined to produce a complete understanding of the 1999 Shishaldin eruption, despite the difficulties associated with accessing such a remote site. In this first paper, we shall discuss the two Strombolian phases and estimate gas volume and pressure at the vent. In a series of papers, we interpret the pre-Subplinian (Vergniolle and Caplan-Auerbach, 2004a, this issue), trends in gas velocity (Vergniolle and Caplan-Auerbach, 2004b), the Subplinian phase (Vergniolle and Caplan-Auerbach, 2004c) and propose a general mechanism to explain the chronology of the entire 1999 Shishaldin eruption (Vergniolle and Caplan-Auerbach, 2004d).

4. Bubble vibration model

During Strombolian activity, the gas pocket is released by foam coalescence at depth and rises in the volcanic conduit. Its violent formation at depth causes an excess of pressure inside the large bubble, resulting in strong initial oscillations (Vergniolle, 1998). The bubble takes a finite time to rise through the conduit, and its motion might be expected to generate acoustic or seismic energy. However, at Shishaldin, the frequent bursting of bubbles at the surface, with inter-event times of less than 10 s, prohibits us from identifying the low amplitude signals associated with bubble rise. Furthermore, the seismic traces were saturated by strong seismic tremor, so seismic signals resulting from bubble rise are also impossible to distinguish. Due to the large liquid viscosity, the long newly formed bubble, rising in a conduit, does not have enough time to equilibrate its internal pressure to the decreasing pressure field (Vergniolle, 1998). When it reaches the top of the magma column, an excess of pressure is kept inside the "about to break" bubble and strong volumetric oscillations at the magma surface ensue. The amplitude of oscillations results in the radiation of sound waves (Vergniolle and Brandeis, 1996; Vergniolle, 2003). The extreme similarity between the waveforms for explosions recorded at Stromboli and Shishaldin volcanoes suggests that the same mechanism is at work (Fig. 3).

4.1. Qualitative description

Bubbles of several meters in diameter have been observed bursting at the vent at Etna (Coltelli et al.,

1998; T. Pfeiffer's photograph, pers. com., 2001). However, the bursting, i.e. the connection of magmatic gas to atmosphere, of such large bubbles produces frequencies around 150 Hz for a radius of 1 m and 30 Hz for a radius of 5 m by analogy to the balloon bursting problem (Temkin, 1981; Vergniolle and Brandeis, 1994). Because frequencies recorded at Shishaldin volcano are ≈ 1 Hz, we propose that its sound is produced by the vibration of a shallow metric bubble prior to bursting, rather than by the popping noise (Vergniolle and Brandeis, 1994, 1996). Any bubble in an infinite liquid oscillates easily: inertia causes the bubble to overshoot its equilibrium radius and the compressibility of gas, through the internal gas pressure, acts like a restoring force (Batchelor, 1967; Leighton, 1994). The experimental study of Kirpatrick and Lockett (1981) indicates that bubbles moving at speeds approaching the terminal velocity upon reaching the free surface, tend to come to rest and bounce a couple of times before bursting. Here, since the bubbles are coming from the depth of the reservoir, their rise speed had enough time to reach its equilibrium value and the bubble vibration at the top of the magma column, which is the volume mode, is the most likely phenomenon to explain the peak in acoustic pressure. Here, we assume that the oscillations are set up by a sudden overpressure inside a large bubble reaching the magma–air interface.

We approximate the bubble shape by a hemispherical head and a cylindrical tail, as expected in slug-flow (Fig. 4). If the lava is close to the surface, as it is the case at Shishaldin (Dehn et al., 2002), no external limitation exists on bubble growth when the bubble reaches the surface and breaks in the much larger area of the crater (Fig. 5).

Although most vents are seen to be funnel shaped (Sparks et al., 1997), the precise shape of the vent at Shishaldin is not well known, and thus we do not consider its exact geometry. We also neglect the amplification of the sound inside a short tube and

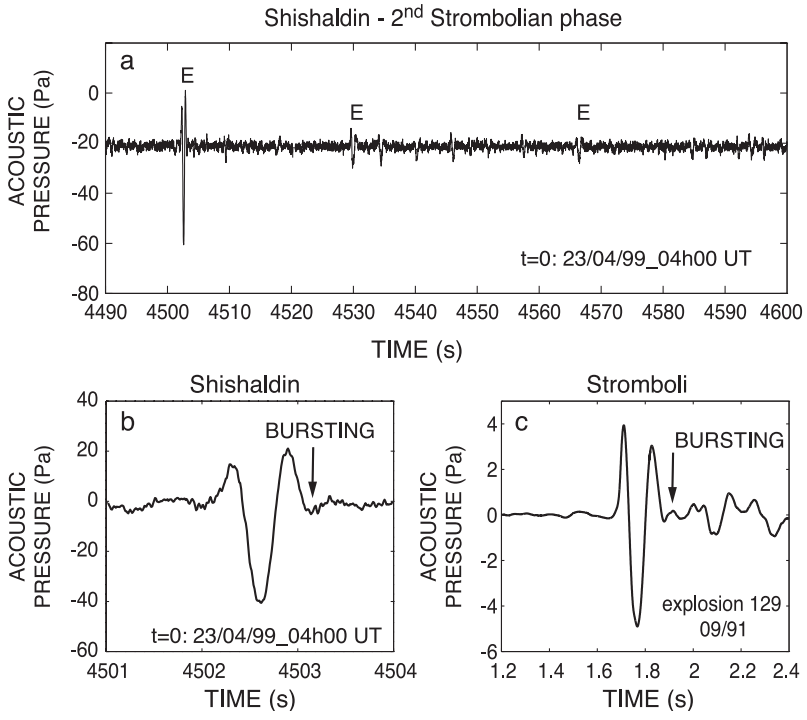

Fig. 3. Time series for Strombolian explosions at (a, b) Shishaldin and (c) Stromboli. E marks where explosions occur. The extreme similarity between the two waveforms encourages us to apply the same acoustic model for both volcanoes. Note that frequencies are different, ≈ 1 Hz at Shishaldin and ≈ 9 Hz at Stromboli. Data in figure a are raw and the mean value of acoustic pressure is removed in figure b.

the distortion due to its propagation from the source to the microphone, as we have shown they are small when recording close to the source (Vergniolle and Brandeis, 1994, 1996). At Shishaldin, there is line-of-sight viewing from the summit to the location of the pressure sensor, and the crater wall is lower in that direction, allowing direct acoustic propagation.

While we cannot rule out the possibility of echoes from the crater walls, the extreme similarity between Shishaldin explosive signals and those observed at other volcanoes suggests that echoes did not contribute significantly to the time series. At the time of Strombolian activity, thermal anomalies in satellite imagery confirm that there was a significant amount of lava within the summit crater (Dehn et al., 2002), suggesting that the bubbles burst near the top of the conduit, and thereby minimising the effects of propagation within the conduit itself.

Because the distance between vent and measurements site is relatively large, about 20 times the wavelength, we have to consider the effects of the propagation of the sound wave in a stratified atmosphere. Because the atmosphere is stratified, the sound speed varies with height and there are regions, at 10–20 and 70–90 km elevation, in which the sound speed is minimum (Garcès et al., 1998a,b). These regions can trap waves and propagation occurs along these ducts without the radial attenuation of a monopole. At Shishaldin, we are concerned with acoustic waves generated at an elevation of 2.85 km above sea level and recorded at 6.5 km. Therefore, a spherical wave reaching the pressure sensor, can attain a maximum height of 9.25 km into the atmosphere, well below the low-velocity zones. Although the addition of a wind field introduces anisotropy in the infrasonic propagation, a wind blowing opposite to the direction of the wave propagation is simply to reduce the effective sound speed (Garcès et al., 1998a,b). Since we will show in next section that the sound speed is ≈ 340 m/s and the radiation approximately that of a monopole, we feel confident that atmospheric effects are not significant. Finally, the aforementioned similarity between Shishaldin explosions and acoustic signals recorded at Stromboli, Etna, Erebus and other volcanoes is a compelling reason to believe that the waveforms are not significantly affected by wind or atmosphere.

A Strombolian bubble reaching the surface is half way immersed into the magma and half way in air, despite a thin layer of magma above it (T. Pfeiffer's photograph, pers. com., 2001; Fig. 4). Because of the large difference in viscosity between air and magma,

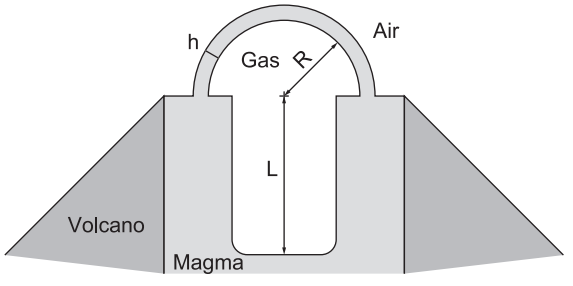

Fig. 4. Sketch of a vibrating bubble at the top of a magma column. *R*, *L* and *h* are, respectively, bubble radius, length and thickness of the magma layer above the bubble.

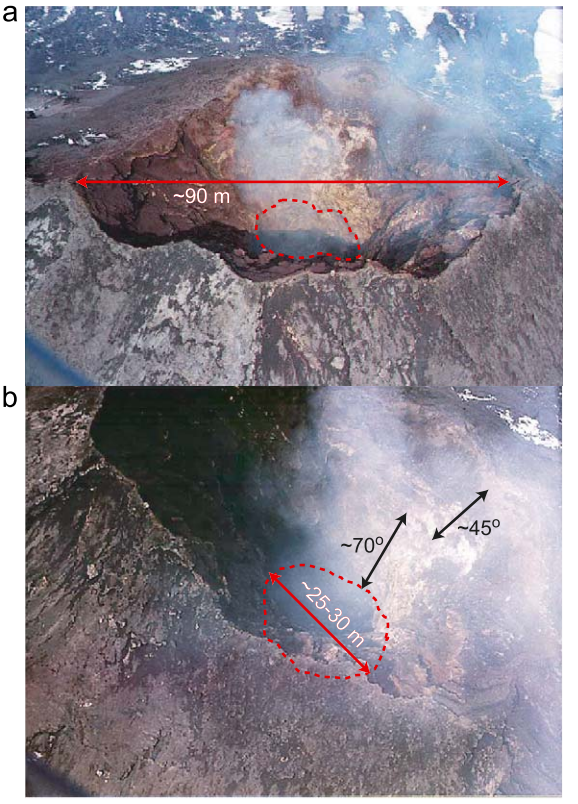

Fig. 5. Two photographs of Shishaldin vent taken by *P. Stelling* (AVO) during an overnight flight of the 16 August 1999. The radius of the conduit mouth was estimated in 2003 by using the shadow of the helicopter on the ground next to the crater.

the motion of the immersed part of the bubble is restricted (Vergniolle and Brandeis, 1994, 1996). Therefore, bubble vibration is entirely concentrated into its hemispherical cap: the magma–air interface vibrates as the bubble does. The thickness of the layer of magma is likely to be of the order of magnitude of the average diameter of the ejecta, as observed on large bursting bubbles. Ejecta, usually a few centimeters thick, are much smaller than the radius of the bubble, which is on the order of 1–5 m (Vergniolle and Brandeis, 1994, 1996). Hence, we will consider this layer as a membrane. The temperature inside the bubble is chosen to be 1323 K (the approximate temperature estimated by Dehn et al. (2002) at the time of Strombolian activity) and the magma will be assumed Newtonian. To estimate the viscosity of Shishaldin magmas, we use geochemical data from Stelling et al. (2002)and Kware magma software (Wohletz, 2001). Using a temperature of 1323 K and a water content of 1.5 wt.% we estimate a viscosity of 500 Pa s. Neither uncertainties on the temperature or viscosity plays a major role in the bubble dynamics at the air–magma interface.

4.2. Equations

The source of sound is a thin layer of magma, pushed by a variation of internal pressure inside the bubble (Vergniolle and Brandeis, 1996). We have shown for Stromboli that the source is a monopole as its amplitude decreases inversely proportional to the distance between the microphone and the vent (Vergniolle and Brandeis, 1994). Similar analysis at Shishaldin is not possible since the network includes only a single pressure sensor. However, we examined the amplitude of ground-coupled airwaves on the Shishaldin seismic network and found that, to first order, the amplitudes of these waves are inversely proportional to distance from the vent. So we feel confident that these explosions are also monopolar and do not propagate into one of the ducted channels of the stratified atmosphere. In this case, the excess pressure depends on the rate of mass outflow from the source, $\dot{q}$ (Lighthill, 1978). Acoustic pressure p_{ac} emitted at the source at time t will reach the microphone, at a time $t+r/c$, where r is the distance r from the vent and c the sound speed in air equal to 340 m/s, as determined by the moveout of airwaves arriving at the various Shishaldin seismic stations. For such a radiation, analogous to a monopole, the excess pressure $p_{ac}-p_{air}$ at time t is (Lighthill, 1978):

$$p_{ac}-p_{air}=\frac{\dot{q}(t-r/c)}{4\pi r}=\frac{d^2}{dt^2}\left[\frac{4\pi R^3(t-r/c)}{6}\right]\frac{\rho_{air}}{2\pi r} \quad (1)$$

where ρ_{air} is air density equal to 0.9 kg/m^3 at an elevation of 2850 m (Batchelor, 1967). Note that factor 2 in the farthest right hand-side of the equation accounts for radiation in a halfspace, whereas a factor of 6 represents half a spherical bubble. Therefore, acoustic pressure is exactly that of a monopole.

The bubble vibrates as a thin membrane of thickness h. Its head grows but remains spherical with a radius R, the normal mode being assumed for simplicity and favored during the bubble expansion. The part of the bubble which remains in the cylindrical tube has a length L (Fig. 4). Hence, the bubble has a volume V_g equal to:

$$V_g=\frac{2\pi R^3}{3}+\pi R_o^2 L \quad (2)$$

where R_o is the initial radius. Note that in the following, indexes o, g and eq refer to initial conditions, gas and equilibrium values, respectively. The high viscosity of magma impedes any significant drainage by gravity of the magma above the bubble, during the short time allowed for the bubble to vibrate. The volume of magma above the bubble is conserved and the liquid stretches, following the variations in bubble radius:

$$R^2h=R_{eq}^2h_{eq}. \quad (3)$$

Because heat transfer inside large bubbles is adiabatic (Plesset and Prosperetti, 1977; Prosperetti, 1986), the pressure p_g inside the bubble follows the variations of its volume V_g with a ratio of specific heat γ, equal to 1.1 for hot gases (Lighthill, 1978). Suppose, for simplicity, that the bubble, initially at rest at the magma–air interface, is suddenly overpressurised by an amount ΔP. The bubble starts to grow and vibrate in response to the pressure change. Pressure and volume obey the adiabatic law, hence we can follow their variations. The bubble radius R can be expressed by its variation

around its equilibrium radius R_{eq} calculated from the initial conditions and the adiabatic law (Vergniolle and Brandeis, 1996):

$$R = R_{eq}(1+\varepsilon) \tag{4}$$

with

$$R_{eq} = \left(\frac{3}{2}\right)^{1/3}\left[\left(\frac{2R_o^3}{3}+R_o^2L\right)\left(1+\frac{\Delta P}{p_{air}}\right)^{1/\gamma}-R_o^2L\right]^{1/3}. \tag{5}$$

The motion of the bubble is possible through an exchange between the kinetic energy of its hemispherical cap and the potential energy inside the gas and the general equation for bubble vibration is:

$$\ddot{\varepsilon}+\left(\frac{12\mu}{\rho_{liq}R_{eq}^2}\right)\dot{\varepsilon}+\frac{p_{air}}{\rho_{liq}R_{eq}h_{eq}}\left[1-\left(\frac{V_{eq}}{V_g}\right)^{\gamma}\right](1+\varepsilon)^2 = 0 \tag{6}$$

where the gas volume V_g is a function of ε (Vergniolle and Brandeis, 1996). Finally, we have to specify two initial conditions. The first one is the initial radial acceleration $\ddot{\varepsilon}_o$, which depends on the initial force applied to the layer of magma. Assuming that the bubble, at rest at the magma–air interface, is suddenly overpressurised by an amount ΔP, this force is directly related to the bubble overpressure. Since the bubble is formed at depth and rises in a tube full of viscous liquid, there is always an disequilibrium between the external pressure field and the gas pressure as a consequence of the significant delay to equilibrate a moving bubble with large viscosity fluids (Vergniolle, 1998, 2001). Therefore, the overpressure at the surface can be viewed as a consequence of either the bubble rise within a viscous magma or its violent formation at depth (Vergniolle, 1998, 2001).

The initial radial acceleration, $\ddot{\varepsilon}_o$ is equal to:

$$\ddot{\varepsilon}_o = \frac{\Delta P R_o^2}{\rho_{liq}R_{eq}^3h_{eq}}. \tag{7}$$

The second initial condition to be specified is the initial radius ε_o:

$$\varepsilon_o = \frac{R_o}{R_{eq}} - 1. \tag{8}$$

Radial acceleration is maximum when the strong vibration starts and, therefore, the initial radial velocity is equal to zero. These initial conditions correspond to a bubble close to its minimum radius.

Bubble radius, velocity and acoustic pressure are calculated for a typical bubble present during the initial period of the second Strombolian phase. For a bubble radius of 5 m, a length of 24 m and an overpressure of 0.15 MPa, the maximum velocity is 30 m/s (Fig. 6). The magma above the bubble starts with a thickness of 0.8 m when the oscillation is set up into the bubble and reaches a minimum at 0.08 m. Damping due to the viscosity, $\mu = 500$ Pa s, is very small (Fig. 6c). The first absolute minimum in acoustic pressure corresponds to the maximum bubble expansion ($R \approx 15.4$ m) and the second following zero in acoustic pressure to the minimum radius (Fig. 6d). Note that the non-linearity of the equations result in an asymmetry between the positive and the negative peak and that acoustic pressure, which depends on acceleration as well on velocity, is at its minimum close to the maximum radius.

The bubble vibration can have a large amplitude and cases are reported where maximum radius is twice the equilibrium radius when the bubble collapse, occurring near its minimum radius, is modelled (Leighton, 1994). Here, at Shishaldin, although the change in bubble radius is large, the maximum radius, ≈ 15.4 m, is less than twice the equilibrium radius, ≈ 11.3 m during the second Strombolian phase (Fig. 6a).

4.3. Description of the model

Direct observations of large bubbles at the top of the magma column are very sparse because the lava is rarely visible at the vent and because viewing such activity is typically dangerous. Although Blackburn et al. (1976) report some bubbles at Heimaey and Stromboli, the short duration of the bubble vibration cycle at the interface, probably between 0.1 and 1 s, makes identification of this vibration difficult at best. Furthermore, the large bubbles present during Strombolian activity are probably of two different types. Strombolian bubbles are those which form in the magma chamber and consequently arrive at the top of the magma column with some residual overpressure. These are strongly overpressurised, break while producing large ejecta velocities and cannot be safely

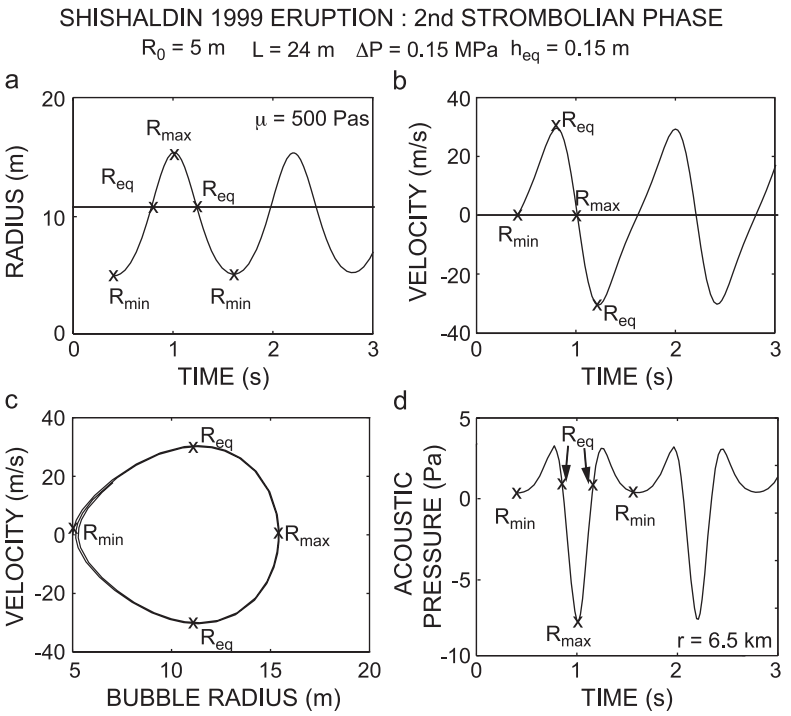

Fig. 6. Time evolution for a characteristic bubble of initial radius $R_0 = 5$ m, length $L = 24$ m, overpressure $\Delta P = 0.15$ MPa, equilibrium thickness above bubble $h_{eq} = 0.15$ m, $\mu = 500$ Pa s. Oscillations start at time equal to 0.4 s. (a) Bubble radius (m). (b) Bubble radial velocity (m/s). (c) Bubble velocity (m/s) as a function of bubble radius (m). (d) Acoustic pressure recorded at 6.5 km from the vent (Pa).

observed. The second type of large bubble corresponds to those formed by local and slow coalescence in the conduit, and has no significant overpressure at the top of the magma column. Although they are difficult to see on acoustic records, due to their lack of gas overpressure, they may correspond to the bubbles observed popping at the vent, which are safe to observe.

Our model for the sound produced at the vent during the Strombolian phases is based on the assumption that the large bubble, lying just below the top of the magma column, is suddenly set with an initial gas overpressure at time t equal zero. Although this assumption is a simplification, once the bubble rises from depth, its internal pressure is never at its equilibrium because the bubble is continuously exposed to a lesser external pressure and the viscosity of the liquid delays the return to equilibrium (Vergniolle, 1998, 2001). As the bubble approaches the top of the magma column, the pressure release increases on the gas inside the bubble, leading to the build-up of a viscous overpressure inside the large bubble (Vergniolle, 1998). Furthermore the formation of the large bubble at the depth of the reservoir from foam coalescence (Jaupart and Vergniolle, 1988, 1989) is violent and an initial overpressure is set in the bubble when it starts rising in the conduit (Vergniolle, 1998). At Stromboli, the initial overpressure at the approximate depth of 300 m, is of the order of 11 MPa (Vergniolle, 1998) in agreement with seismic studies (Chouet et al., 2003). However calculations of the exact physical behaviour of the large bubble close to the top of the magma column are very complex and are left to further studies.

There are many papers which discuss the behaviour of a pulsating bubble in a infinite liquid (Leighton, 1994). Our equations are fairly similar to Rayleigh-Plesset equations (Plesset and Prosperetti, 1977; Prosperetti, 1986; Leighton, 1994), although they are adapted for the vibration of a bubble close to an interface between a liquid (magma) and a gas (air

at atmospheric pressure). In these papers, the scaling for the oscillation amplitude is done on the bubble maximum radius, but our scaling on its equilibrium radius is strictly equivalent (Eq. (4)). A bubble pulsating at finite amplitude, as here with the maximum dimensionless radius $\varepsilon \approx 0.36$ (Eq. (4)), is clearly a non-linear oscillator as shown by its trajectory phase (Fig. 6c). There is an obvious asymmetry: while in expansion the amplitude of the bubble wall displacement has no absolute limit, in compression the radial displacement of the wall from equilibrium cannot be greater than the equilibrium radius (Leighton, 1994). Surface tension and viscosity have a significant effect on the dynamics of microbubbles but are less effective in maintaining a spherical shape for the large Strombolian bubbles described here. Consequently, the bubbles experience shape distortions and oscillations due to overshooting (Leighton, 1994). At Shishaldin, the shape of the large bubble is confined by the conduit walls to be cylindrical with a nose whose shape results from the potential flow of liquid around its tip (Batchelor, 1967; Wallis, 1969). Furthermore, the large viscosity of the magma around the bubble slows down the potential deformations and the initial overpressure, existing in the bubble once oscillations are set, favors a spherical bubble cap during its expansion.

Large bubbles have been produced by underwater chemical explosions using explosive charges and the largest charge can generate a bubble with a maximum radius of 10 m. The maximum radii of bubbles produced by underwater nuclear explosions are of the order of 100 m (Leighton, 1994). After expanding to their maximum size as a result of an explosion, the bubbles oscillate at least for several cycles before reaching the sea surface (Batchelor, 1967; Leighton, 1994). For underwater explosions, the resulting bubble oscillates for a few cycles between a minimum radius of 5 m and a maximum of 18 m (Cole, 1948). We envision a similar mechanism for Shishaldin bubbles, although there the origin of oscillations is obviously quite different.

Our model assumes that the magma above the bubble has a constant volume during the duration of one cycle, i.e. ≈ 1 s. However, the thin liquid film above the bubble is both pulled down by gravity and slowed down by the viscous force within the film of magma. For simplicity and although the bubble nose is half a sphere, we assume that the flow occurs on a vertical wall by gravity, providing a maximum bound on the drainage velocity V_{dr}. The free fall of a thin liquid film of thickness δ onto a vertical solid wall has a velocity of (Wallis, 1969):

$$V_{dr} = \frac{\rho_{liq} g \delta^2}{3\mu} \tag{9}$$

where $\mu \approx 500$ Pa s is the magma viscosity at Shishaldin and $\rho_{liq} \approx 2700$ kg/m^3 the magma density. The characteristic drainage time τ_{dr} is the ratio between the characteristic bubble radius $R_o \approx 5$ m and the drainage velocity based on the equilibrium thickness $\delta \approx h_{eq}$:

$$\tau_{dr} = \frac{R_o}{V_{dr}}. \tag{10}$$

Although the drainage velocity is largely overestimated, the drainage time τ_{dr} is larger than 12.6 s for an equilibrium thickness $h_{eq} = 0.15$ m. This is one order of magnitude above the characteristic time for vibration, ≈ 1 s, confirming that drainage is therefore negligible during the bubble vibration at the top of the magma column.

Acoustic measurements suggest that a Strombolian bubble sustains one cycle of oscillation before breaking. This is possible if the radial stress σ_{rr} and the tangential stresses $\sigma_{\theta\theta}$ and $\sigma_{\phi\phi}$ do not exceed the mechanical strength of the magma. For a bubble of radius R_o surrounded by a thin magma shell of thickness h_{eq}, the stresses are:

$$\sigma_{rr} = \Delta P_g / 2 \tag{11}$$

and

$$\sigma_{\theta\theta} = \frac{\Delta P_g R_o}{2 h_{eq}} \tag{12}$$

where ΔP_g is the gas overpressure (Landau and Lifshitz, 1986), here assumed to be equal to the initial gas overpressure, ΔP. The smallest of the three stresses are the tangential ones, equal to 25 MPa, for the maximum overpressure recorded during the two Strombolian phases, ≈ 1.4 MPa, a bubble radius of 5 m and a film thickness of 0.15 m. Because the tensile strength of magma, 320 MPa (Dingwell, 1998), is more than 10 times larger than the applied stress, the magma layer

above the Strombolian bubbles at Shishaldin is mechanically stable and will not fail. Therefore, the bubble can vibrate and does not pop. The model of bubble vibration before breaking is in excellent agreement with the measured frequency, which is more than an order of magnitude below the frequency of a bursting balloon, i.e. a bubble whose liquid film is stretched beyond its elasticity towards bursting. Furthermore, the simplified model for a balloon bursting produces a waveform of the acoustic pressure, which corresponds to a N-Wave, i.e. with both a very strong rising time and the same amplitude for the positive and negative peaks (Temkin, 1981). These two features are not observed in the Shishaldin acoustic record.

The second mechanism by which such a large and overpressurised bubble can break is by developing instabilities at the magma–air interface or the magma–bubble interface. If the gas–liquid interface is a plane surface, the interface is stable only when the acceleration is directed from the liquid to the gas phase. However, the stability of a spherical surface depends not just on its acceleration but on its velocity: during bubble growth the streamlines diverge and produce a stabilising effect, while the reverse happens during contraction (Plesset and Mitchell, 1956; Leighton, 1994). Although the bubble nose is only half a sphere, we use the stability analysis for a sphere and the bubble wall interface is stable if the stability factor C_{RT}:

$$C_{RT} = \frac{(n-1)(n+1)(n+2)\sigma}{\rho_{liq} R_o} - \frac{3\dot{R}}{4R_o^2} - \frac{(2n+1)\ddot{R}}{2R_0} \quad (13)$$

is greater than zero. n is the order of the harmonic, σ the surface tension, R_o, $\dot{R}$ and $\ddot{R}$ are, respectively, the bubble radius, bubble radial velocity and bubble radial acceleration (Plesset and Mitchell, 1956; Leighton,

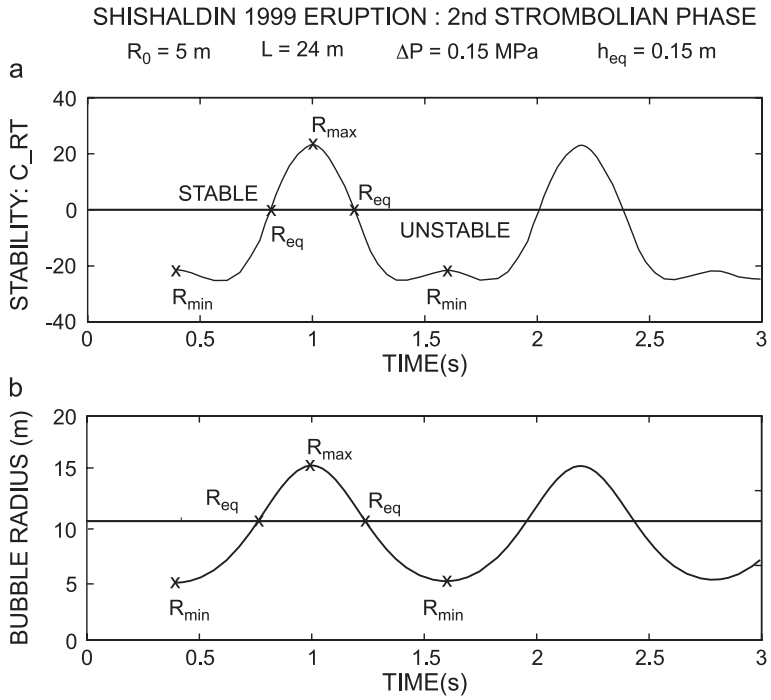

Fig. 7. (a) Stability of the bubble wall interface and (b) bubble radius (m) in time (s) for a typical bubble of the second Strombolian phase, with initial bubble radius R_0 of 5 m, bubble length of 24 m and initial overpressure of 0.15 MPa. Magma thickness above bubble h_{eq} is 0.15 m and magma viscosity μ is 500 Pa s. Oscillations start at time equal to 0.4 s and the bubble wall interface is unstable if the coefficient C_{RT} is negative, i.e. around the minimum radius.

1994). The surface tension term, with $\sigma \approx 0.36$ kg/s^2 for a basaltic magma at 1200 °C and 0.1 MPa (Proussevitch and Kutolin, 1986; Proussevitch and Sahagian, 1996), can be ignored for bubbles as large as a few meters. The perturbation of a spherical surface would remain small for $1 \geq R/R_{max} \leq 0.2$ and will become violent for $R \leq R_{max}/10$. For a typical bubble of the second Strombolian phase, of radius, length and overpressure of respectively 5 m, 24 m and 0.15 MPa, the bubble is potentially unstable for about 1 s around its minimum radius (Fig. 7). Although the bubble also appears unstable for the first 0.4 s, this is a consequence of assuming that the bubble oscillation is set at time zero by a sudden overpressure. The ratio between the minimum and the maximum radius, ≈ 0.3, shows that the instability, occurring close to the minimum radius, is mild for Shishaldin bubbles. Although viscous effects will delay the growth of the instability occurring on the bubble wall near its minimum radius, acoustic data shows that the bubble vibration probably lasts just slightly more than one cycle.

5. Generation of synthetic waveforms

Two main periods of Strombolian activity at Shishaldin volcano were recorded by the pressure sensor: on April 19 from 20:26 h to midnight (first Strombolian phase) and from 12:00 h the 22nd of April to 12:00 h the 23rd of April (second Strombolian phase). During the quiet period in between, some signals, also attributed to breaking bubbles, were detected (Thompson et al., 2002; Caplan-Auerbach and McNutt, 2003) but are ignored here due to poor signal strength.

Due to the enormous quantity of explosions, we selected the largest explosion during a given time period for waveform modelling. This period was taken as 400 s for the first Strombolian phase and 800 s for the second one, for a total of 29 and 106 analysed explosions respectively. For each selected explosion of the two Strombolian phases, a best fit between a synthetic waveform and acoustic measurement is performed manually. In generating synthetic waveforms there are four parameters that are adjusted to determine the best fit model: bubble radius, magma film thickness, bubble length and bubble overpressure. Of these parameters, we choose to fix the values for bubble radius and magma film thickness at 5 and 0.15 m, respectively, allowing bubble length and overpressure to vary. The comparison between model and data is extremely good for the first cycle of bubble vibration and is not valid after the bubble bursts (Fig. 8). Here, we discuss the assumptions associated with these parameters and the effect on our results of varying them.

5.1. Thickness of the magma layer, h_{eq}, above bubble

In previous studies of Strombolian explosions, the thickness of magma above the vibrating bubble, h_{eq}, has been scaled by the average diameter of ejecta (Vergniolle and Brandeis, 1996). Photographs of magmatic bubbles breaking at the surface of magma, are in very good agreement with this assumption. At Stromboli, this has lead to very reasonable values of bubble overpressure, and length, between 2 and 20 times the bubble radius, as expected for slug flow (Wallis, 1969). At Etna, a value of $h_{eq} = 0.1$ m gives very reasonable results for the bubble length and overpressure (Vergniolle, 2003). Shishaldin deposits, however, yield few clues as to the size of the Strombolian ejecta. Maximum clast sizes in Shishaldin

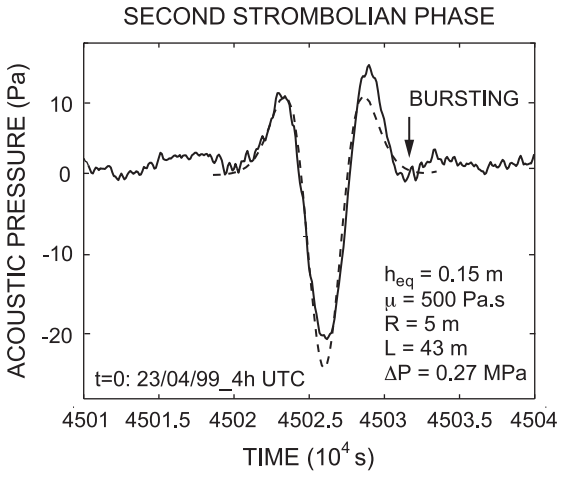

Fig. 8. Comparison between measurements of acoustic pressure (plain line) and synthetic waveform (dashed line) for one explosion of the second Strombolian phase. The synthetic acoustic pressure is produced by a bubble of radius $R_0 = 5$ m, length L of 43 m and an overpressure ΔP of 0.27 MPa. Bubble bursting probably occurs after one cycle of vibration.

tephra samples range from 0.5–22 cm (Stelling et al., 2002), but no distinction can be made between deposits ejected during the Strombolian and Subplinian phases. Synthetic waveforms, however, suggest that a value of 0.15 m is appropriate for Shishaldin explosions, an approximation that we investigate below.

Since we have little information on the size of Strombolian ejecta, and hence the thickness of the magma layer above the bubble, we assume that the equilibrium thickness is the same for all bubbles during the two Strombolian phases. Synthetic waveforms are very sensitive to the thickness of magma above the breaking bubble because it represents the mass of the oscillator. At Shishaldin, using a thickness of magma outside of the range 0.1–0.2 m leads to unreasonable values of either bubbles length and overpressure. For example, a typical explosion of the second Strombolian phase can be fit by using a film thickness of 0.15 m and a bubble radius, length and overpressure of respectively 5 m, 24 m and 0.15 MPa (Fig. 6). If the film thickness is doubled, the bubble radius and length are halved to 2.5 and 10 m, respectively. However, the initial overpressure is multiplied by 6, giving 0.9 MPa at the vent, which is more typical of an explosive volcano than one with an open conduit. Thus, a 0.30 m thick film would require unrealistic overpressures for this phase. Secondly, the radial oscillation of the bubble cap can only be excited when the thickness of the liquid above the bubble is small compared to its radius, so the bubble can produce a dome over the liquid. For a film of equilibrium thickness of 0.3 m, the magma thins from 1.5 to 0.11 m for a bubble radius of only 2.5 m (Fig. 9) invalidating the requirement that the film is small compared to the bubble radius.

Finally, although a thickness h_{eq} equal to 0.2 m matches most of the explosions, it failed for the relatively "highest" frequencies measured on the 23rd of April. A value of h_{eq} equal to 0.1 m can produce a reasonable match between synthetic waveforms and measurements but leads to extremely long bubbles, of a length above 20 times the radius. We have no observations favouring extremely long bubbles, since fire fountaining was not observed during the Strombolian phases. Therefore, a value of 0.15 m for the magma thickness above each bubble, h_{eq}, is chosen for all explosions at Shishaldin volcano.

Because the bubble breaks when its radius is close to its minimum value, the liquid film is at its largest, with a value close to 0.8 m when the bubble breaks. However, since the mechanism of breaking is related to an instability, the size of the ejecta will probably be of the order of the wavelength of the instability, i.e. of the order of the equilibrium thickness and not its maximum thickness. Thus, there is no conflict with the thickness of the film at the breaking point and the size of the ejecta.

5.2. Constraints on bubble radius

Laboratory experiments show that in well-developed slug flow, bubbles occupy a large portion of the conduit (Jaupart and Vergniolle, 1988, 1989). Consequently, unless the shape of the conduit changed significantly during the eruption, it is reasonable to expect that the bubble radius would remain approximately constant throughout the 1999 eruption.

Synthetic waveforms modelling Shishaldin bubbles suggest that all of the bubbles have a radius of $\approx$ 5 m. A bubble radius of 5 m, and a conduit of 6 m, is supported by observations of the top of the Shishaldin conduit. Photographs taken in August 1999 and July 2003, during overflights of the vent (Fig. 5) show the top of a vertically walled conduit, the radius of which is estimated to be $\approx$ 12–15 m. In the latter flight, the shadow of the helicopter on the crater wall was used as a measuring tool to constrain the vent radius. In both instances, only the top several meters can be seen in the photo (Fig. 5), but we assume that it tapers at depth and has a funnel shape as most of the observed vents (Sparks et al., 1997). Our estimate of a 6 m radius is also consistent with direct observations of active vents at Etna volcano, 1–5 m (Le Guern et al., 1982; Calvari et al., 1994; Coltelli et al., 1998; Vergniolle, 2003) and at Kilauea volcano ($\approx$ 10 m; Richter et al., 1970; Wolfe et al., 1987) and is larger than that seen at Stromboli volcano ($\approx$ 1 m; Chouet et al., 1974). Thus, a conduit radius of $\approx$ 6 m seems reasonable for Shishaldin.

The conduit radius R_c can also be estimated from the initial bubble radius R_o and from the thickness δ of the magma present between the bubble and the solid wall, called the lateral film. If we assume that the

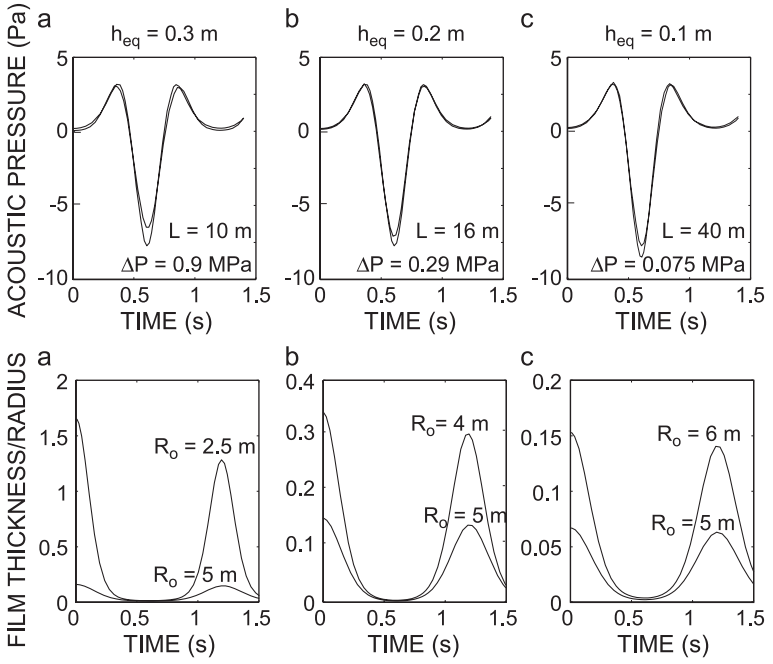

Fig. 9. Sensitivity analysis for various equilibrium thickness, $h_{eq}=0.3$ m for the right column, $h_{eq}=0.2$ m for the middle column, $h_{eq}=0.1$ m for the left column. Acoustic pressure is displayed on the top graphs and ratio between magma thickness and bubble radius R_0 on the bottom graphs. Note that the two graphs on the three top diagrams correspond to the cases shown in the graph below. The right column corresponds to bubble radius $R_0=2.5$ m, length $L=10$ m and bubble overpressure $\Delta P=0.9$ MPa. For the middle column, $R_0=4$ m, $L=16$ m and $\Delta P=0.29$ MPa. In the left column, $R_0=6$ m, $L=40$ m and $\Delta P=0.075$ MPa. Note that there is hardly any difference in acoustic pressure relative to reference case, $R_0=5$ m, $L=24$ m and $\Delta P=0.15$ MPa, $h_{eq}=0.15$ m.

thickness δ has reached its asymptotic value δ_∞, it can be calculated as (Batchelor, 1967):

$$\delta_\infty = 0.9R_c\left(\frac{\mu^2}{\rho_{liq}^2 R_c^3 g}\right)^{1/6}. \quad (14)$$

For a magma viscosity of 500 Pa s and a bubble radius of 5 m, the vertical film δ_∞ around each bubble is ≈ 0.86 m (Eq. (14)). Because the asymptotic value δ_∞ is seldom attained even for long bubbles (Fabre and Linné, 1992) and corresponds to a minimum value, the conduit radius can be safely estimated at ≈ 6 m from acoustic measurements.

We propose that the bubble radius is constant since we assume that the bubble volume fills the width of the tube and there is only one active vent at the summit (Fig. 5). The fairly well peaked frequency range during the whole of the eruption supports this assumption. If we suppose that the thickness of the magma above the bubble is constant and equal to 0.15 m, the measured waveform can be matched by a bubble radius, length and overpressure of respectively 4 m, 27 m and 0.18 MPa or by a bubble with radius of a 6 m, 22 m and 0.13 MPa overpressure (Fig. 10).

Enlarging the possible range of values for the initial bubble radius makes the radial oscillations of the bubble unlikely. When using these two extreme conditions for the bubble radius, the gas volume at atmospheric pressure is known with an accuracy better than $\pm 20\%$. Therefore, a bubble radius of 5 m generates the best synthetic waveforms regardless of when the signal is chosen during the two Strombolian phases. The uncertainties on the bubble radius are probably around 1 m at most if we suppose that the thickness h_{eq} of magma above the bubble is properly determined.

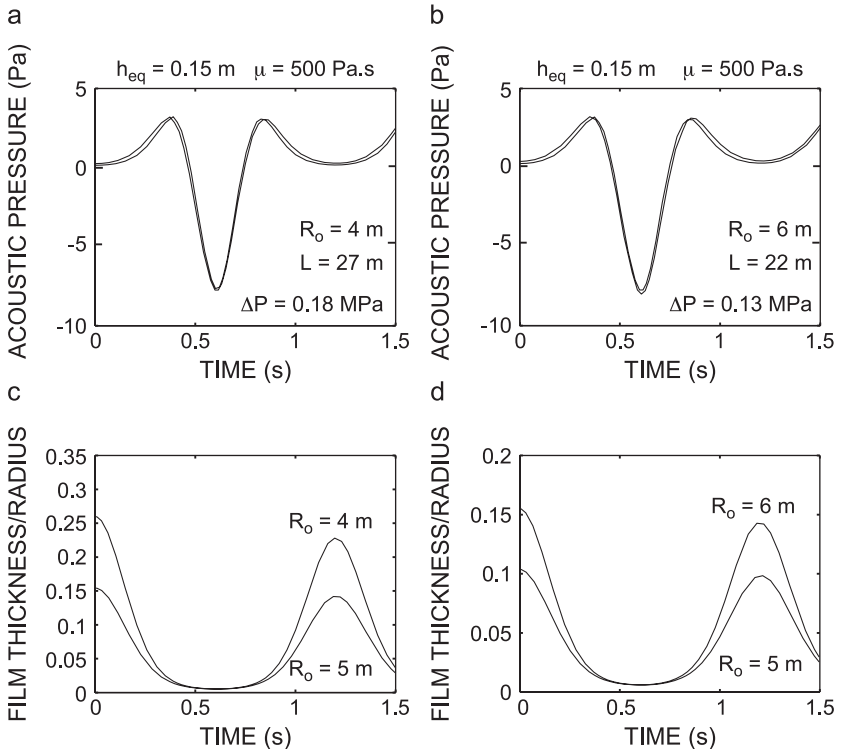

Fig. 10. Sensitivity analysis for various bubble radius $R_0 = 4$ m for the right column, $R_0 = 6$ m for the left column. Acoustic pressure is displayed on the top graphs and ratio between magma thickness and bubble radius R_0 on the bottom graphs. All the graphs corresponds to a constant equilibrium thickness, $h_{eq} = 0.15$ m and a magma viscosity of 500 Pa s. The right column corresponds to bubble length $L = 27$ m and bubble overpressure $\Delta P = 0.18$ MPa. In the left column, $L = 22$ m and $\Delta P = 0.13$ MPa. Note that there is hardly any difference in acoustic pressure relative to the reference case, $R_0 = 5$ m, $L = 24$ m and $\Delta P = 0.15$ MPa, $h_{eq} = 0.15$ m.

5.3. Constraints on bubble length

When a long bubble breaks, such as during a Strombolian explosion, the duration of gas expulsion depends on the gas velocity and the bubble length. If the gas is expelled at a velocity deduced from height measurements (≈ 50 m/s), a 100-m long bubble could produce sound for 2 s, which could be measured on acoustic records. However, the sound produced by a steady gas jet carrying solid fragments is a dipolar source, which radiates sound with less efficiency than a monopole source such as a Strombolian explosion (Woulff and McGetchin, 1976). It is even worse in term of sound radiation if the sound is produced by a gas phase free of solid fragments, a quadrupole source resulting of turbulence in the gas jet itself. Measurements of acoustic pressure, recorded at 6.5 km from the vent and with potentially some wind, do not show any sign of an signal induced by the gas jet itself. Therefore, no constraint can be provided on bubble length.

6. Main results

6.1. Bubble length and overpressure

It is now possible to look at the evolution of bubble characteristics during the two Strombolian phases to constrain the dynamics of the eruption.

The first Strombolian phase (April 19, 1999), which occurs almost immediately after the Subplinian phase, displays no noticeable time evolution in bubble length or overpressure (Fig. 11). Although the bubbles are long (82 ± 11 m), their lengths are less than 20 times the bubble radius, as is expected for slug flow (Wallis, 1969). Bubble overpressures are relatively small,

around 0.083 ± 0.03 MPa. The end of this phase is difficult to see because acoustic signals decrease slowly before falling below the noise level.

The second Strombolian phase (22nd and 23rd of April 1999; Fig. 12) shows more variation than the first (Fig. 11). Bubble lengths, between 10 and 60 m, are still less than 20 times the bubble radius. Bubble overpressure during the second Strombolian phase (Fig. 12) starts and stays at a relatively low value (0.15 MPa), for the first 17 h. It presents a peak at 1.4 MPa on the 23rd of April between 04:40 and 10:13 h, although there is no associated change in the number of events.

While none of these explosions was visually observed, tremor amplitude at the time of the pressure peak on April 23 was the strongest ever recorded by AVO (Thompson et al., 2002). Although no visual observations were made of the Strombolian explosions, satellite imagery at 05:30 h shows a small ash plume, and video taken of the Shishaldin vent at 21:30 h shows the development of another small plume. These can be either the combined effects of frequently breaking, very long, overpressurised bubbles, as shown by the increase in surface flux ≈ 6000 m^3/s (Fig. 15) or proper ash plumes, as shown developing during the pre-Subplinian and the Subplinian phases (Vergniolle and Caplan-Auerbach, 2004b,c).

Here, we propose that the peak in overpressure corresponds to large Strombolian bubbles rising through a gas-rich magma. Laboratory experiments show that under different conditions in the reservoir, a variable quantity of small bubbles is released in the conduit (Fig. 13), which depends on the foam dynamics at the top of the reservoir and its lateral spreading. When the latter is relatively strong, the liquid in the tube is very rich in small bubbles, which rise as an annular curtain of small bubbles (Fig. 13c).

The consequence is that the apparent viscosity of a bubbly magma is much greater than the viscosity of a

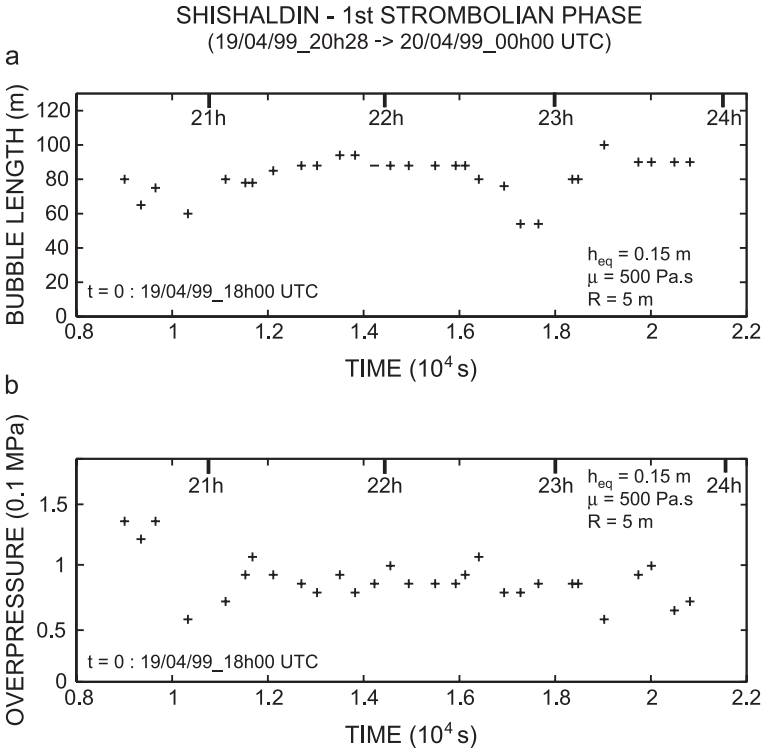

Fig. 11. Results of synthetic waveforms on the largest explosion per 400 s during the first Strombolian phase of the 19th of April 1999. Bubble radius R_0 is 5 m, magma thickness above bubble h_{eq} is 0.15 m and magma viscosity μ is 500 Pa s. Time $t = 0$ is 18:00 h on 19/04/1999 (UTC). (a) Bubble length at the surface (m). (b) Bubble overpressure at the surface (× 0.1 MPa).

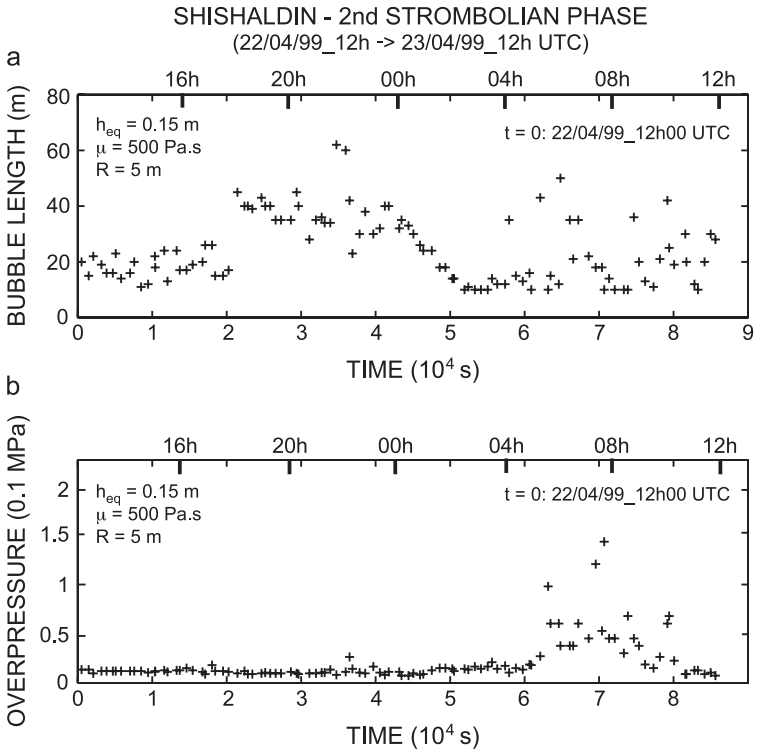

Fig. 12. Results of synthetic waveforms on the largest explosion per 800 s during the second Strombolian phase of the 22nd and 23rd of April 1999. Bubble radius R_0 is 5 m, magma thickness above bubble h_{eq} is 0.15 m and magma viscosity μ is 500 Pa s. Time $t=0$ is 12:00 h on 22/04/1999 (UTC). (a) Bubble length at the surface (m). (b) Bubble overpressure at the surface ($\times$ 0.1 MPa).

magma without bubbles (Jaupart and Vergniolle, 1989). Since the large bubbles of the Strombolian phase come from the depth of the reservoir and are formed with an initial overpressure, their final overpressure at the surface strongly depends on the viscosity of the mixture in which they are rising (Vergniolle, 1998).

The average bubble length, during the second Strombolian phase (24 ± 12 m) is less than a third of the length estimated for the first Strombolian phase. The bubble overpressure during the first 17 h of the second one (Fig. 12) is twice that recorded during the first Strombolian phase (Fig. 11). These differences in bubble lengths and bubble overpressures support the interpretation that the first Strombolian phase results from a strong decompression induced by the Subplinian phase (Vergniolle and Caplan-Auerbach, 2004c,d) whereas the second one is more typical of a classical basaltic eruption with relatively small (0.15 MPa) overpressure. The peak in overpressure is probably the consequence of a magma in the conduit richer in small gas bubbles as shown in the laboratory experiments (Fig. 13c).

6.2. Gas volume and gas flux

Given bubble radius, length and overpressure during the two Strombolian phases, it is fairly easy to calculate the gas volume and gas flux emitted at the surface per bubble. Gas volume and gas flux, calculated at atmospheric pressure, are fairly constant during the first Strombolian phase and are respectively $1.3 \times 10^4 \pm 0.2 \times 10^4$ and $2.9 \times 10^3 \pm 4.1 \times 10^2$ m^3/s (Figs. 14 and 15).

For the second Strombolian phase, we observe a peak between 04:40 and 10:13 h UT ($\approx 1.4 \times 10^4$ m^3 for gas volume ejected per bubble and $\approx 3.8 \times 10^3$ m^3/s for the gas flux) following a 17-h quiet period at $4.7 \times 10^3 \pm 1.9 \times 10^3$ and $1.0 \times 10^3 \pm 4.7 \times 10^2$ m^3/s (Fig. 15). Gas volume and gas flux average for the whole second Strombolian phase is $0.9 \times 10^4 \pm$

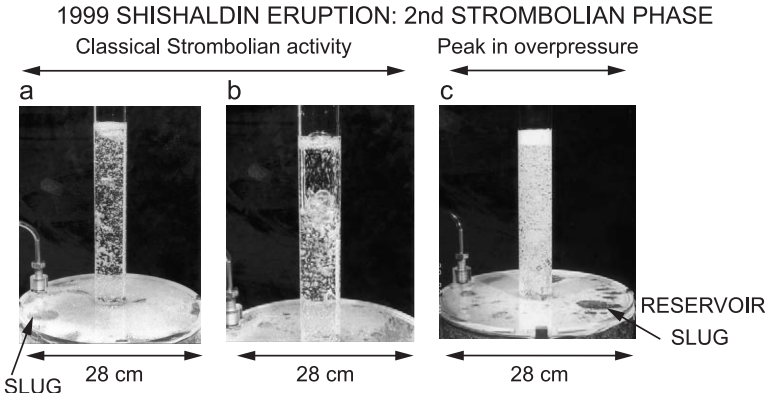

Fig. 13. Laboratory experiments showing that the conduit can contain a small gas volume fraction (a, b) or a relatively large gas volume fraction with a small foam lying on the top of the liquid (c). Liquid is a silicone oil (Rhodorsil) of viscosity 0.1 Pa s (a, b) and 0.01 Pa s (c) for a gas flux of 3.0×10^{-5} m^3/s (a, b) and 1.3×10^{-5} m^3/s. The conduit diameter is 4.4 cm and the number of bubbles at the base of the reservoir is 185. (a) Foam at the top of the reservoir (white part) has started to coalesce (black part on the left-hand side) to produce a slug, i.e. a large gas bubble. (b) Large gas bubble in the conduit, similar to classical Strombolian explosions. (c) Foam at the top of the reservoir (white part) has started to coalesce (black part on the right-hand side) and is about to produce a large bubble, which then will migrate in a conduit rich in small bubbles. Note that there is a permanent foam layer staying at the top of the liquid. This is the laboratory equivalent of the second Strombolian phase during its peak in overpressure.

0.8×10^4 and $2.2 \times 10^3 \pm 1.6 \times 10^3$ m^3/s. If we assume that CO_2 is the major component of the gas, the mass flux is equal to 1.2×10^3 and 8.7×10^2 kg/s for the first and the second Strombolian phases. Mass flux has a minimum value of 470 and 360 kg/s in the endmember case of a pure H_2O phase.

The total gas volume is estimated by counting the number of explosions per 400 s for the first Strombolian phase and per 800 s for the second Strombolian phase. On average one explosion occurs each 8.7 s for the first Strombolian phase and each 12 s for the second one (Caplan-Auerbach and McNutt, 2003). The total gas volume ejected at atmospheric pressure is 3.3×10^7 m^3 for the first Strombolian phase and 1.0×10^8 m^3 for the second. We have seen before that although there are a few simplifying assumptions, the determination of gas volume, and hence gas flux is known with an accuracy of $\pm$ 20% in the framework proposed by the model of bubble vibration.

The number of bubbles has been estimated by counting any bubble with acoustic pressure above the detection limit ($\approx$ 0.5 Pa). The total gas volume and gas flux given above, were estimated using the volume of the largest bubble and the number of events above the detection threshold. The total volume of the smallest detectable bubbles released at atmospheric pressure is $\approx 1.1 \times 10^7$ and $\approx 5.0 \times 10^7$ m^3 during the first and second Strombolian phase. If the distribution of gas volumes follows a gaussian law, the average gas volume is the mean between the minimum and the maximum gas volume, $\approx 2.3 \times 10^7$ and $\approx 7.7 \times 10^7$ m^3 for the first and second Strombolian phase. Gas flux based on that method are reduced by a factor of 0.67 and 0.74 during the first and second Strombolian phases.

Note that the sensitivity, used in this paper, for the pressure sensor is the theoretical value, 0.36 mV/Pa. If instead we use the uncalibrated value of 0.2 mV/Pa, the data amplitudes are multiplied by 0.56. Because the frequency of the signal is not affected by the calibration, the bubbles have the same characteristics in size but gas overpressure increases by 1.8. This leads to a maximum in overpressure of 2.5 MPa for a mean around 0.14 MPa during the second Strombolian phase. Gas volume and gas flux at the surface increase by less than 20%. Therefore, the results present in this paper are fairly robust, except for the gas overpressure during Strombolian explosions, and do not rely heavily on the exact value of the sensitivity.

7. Gas velocity from acoustic power

Thus far we have discussed a model for acoustic measurements based on synthetic waveforms. How-

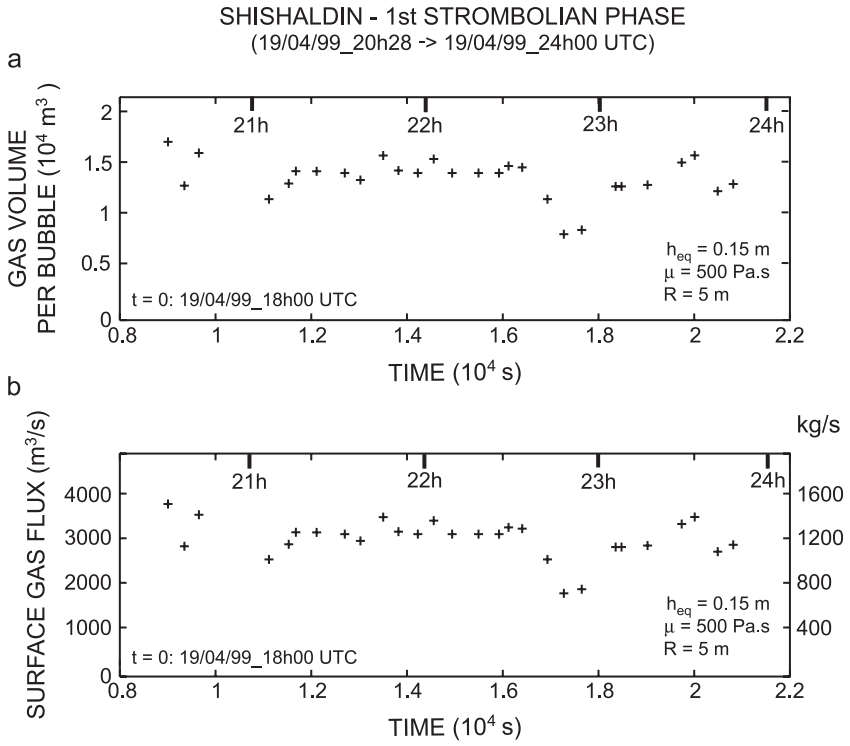

Fig. 14. First Strombolian phase: (a) gas volume ejected by the largest explosion every 400 s and calculated at atmospheric pressure ($m^3\ s^{-1}$) and as mass flux (kg/s) assuming a pure CO_2 phase. Bubble radius R_0 is 5 m, magma thickness above bubble h_{eq} is 0.15 m and magma viscosity μ is 500 Pa s. Time $t=0$ is 18:00 h the 19/04/1999 (UTC).

ever, there might be cases where the quality of acoustic measurements or the intrinsic character of the signal, prevent us from producing synthetic waveforms. We propose a new method, which overcomes that difficulty and allows estimates of gas velocity. We can then compare these results with the results obtained from synthetic waveforms to validate a simple and robust method to obtain gas velocity and gas volume at the vent.

Eq. (6), which describes the time evolution of bubble radius, is required to calculate gas velocity from synthetic waveforms. The maximum velocity of the magma layer above the bubble is found to be $\approx$ 30 m/s for the first 17 h and can reach up to 70 m/s during the final 4-h climax (Fig. 16). This velocity is that of the magma layer and can be smaller than the gas velocity once the bubble has broken. Visual observations by pilots show that ejecta reached heights of a few hundreds of meters earlier on the same day (Nye et al., 2002). If velocity v is simply related to height H by $v=\sqrt{2gH}$ (Wilson, 1980; Sparks et al., 1997), ejecta velocity is between 45 and 70 m/s. Although visual observations were not made at exactly the time during which the pressure sensor recorded Strombolian explosions, there is an order-of-magnitude agreement between explosion waveforms and observed ejecta.

Woulff and McGetchin (1976) have suggested that acoustic power could be used to estimate gas velocity during volcanic eruptions. The total acoustic power, in Watts, emitted in a half sphere of radius equal to the distance r between the vents and the microphone, here 6.5 km, and radiated during a time interval T, is equal to:

$$\Pi = \frac{\pi r^2}{\rho_{air} c T} \int_0^T |p_{ac} - p_{air}|^2 dt \qquad (15)$$

where $\rho_{air}=0.9\ kg.m^{-3}$ at 2850 m elevation (Batchelor, 1967) and $c=340$ m/s is the sound speed (Light-

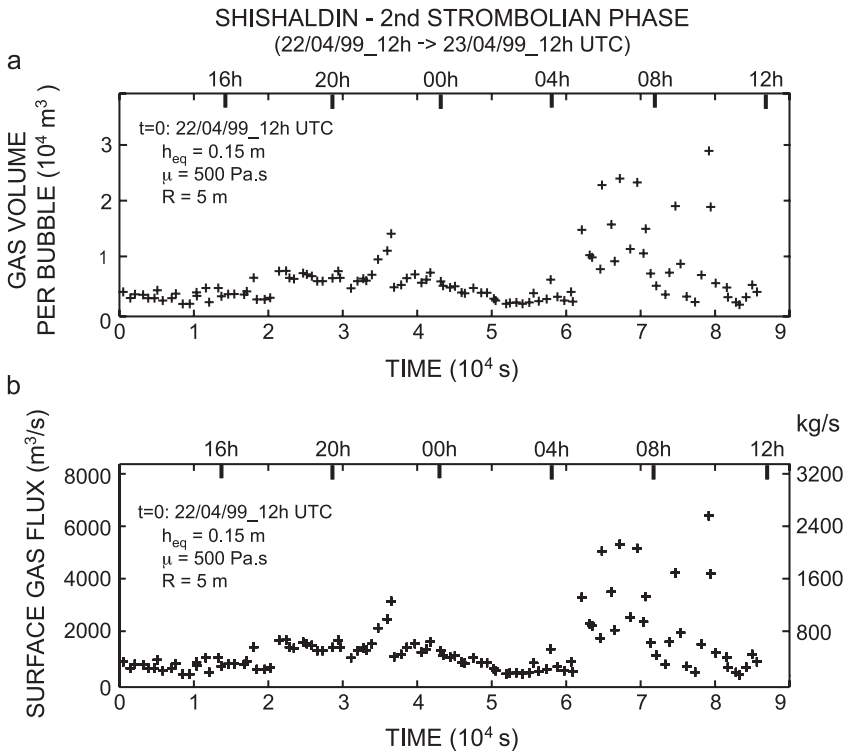

Fig. 15. Second Strombolian phase: (a) Gas volume ejected by the largest explosion every 400 (b) Gas flux ejected by the largest explosion every 400 s and calculated at atmospheric pressure ($m^3\ s^{-1}$) and as a mass flux (kg/s) assuming a pure CO_2 phase. Bubble radius R_0 is 5 m, magma thickness above bubble h_{eq} is 0.15 m and magma viscosity μ is 500 Pa s. Time $t=0$ is 12:00 h the 22/04/1999 explosion every 400 s and calculated at atmospheric pressure (m^3).

hill, 1978). Acoustic power can be then easily measured from acoustic records. However, the relationship between acoustic power and gas velocity depends strongly on the source of sound, which can be monopole, dipole or quadrupole. A monopole source, which radiates isotropically, corresponds to a varying mass flux without external forces or varying stress. For a dipole source, there is a solid boundary which provides an external force. For a quadrupole source, there is a varying momentum flux which acts on the flow. In each case, it is possible to calculate acoustic power by assuming that the signal is periodic and monochromatic with a radian frequency ω and potentially add the contribution of every frequency in a simple linear way.

The source of volcanic explosions has been shown to be a monopole (Vergniolle and Brandeis, 1994). For a monopole source, the excess pressure depends on the rate of mass outflow from the source, $\dot{q}$ in equation (see Eq. (1)). If we assume monochromatic oscillations of frequency ω, $\dot{q}$ has the same dimension as ωq. The two are strictly equivalent if oscillations are small. This simplification gives an order of magnitude for acoustic power. Temkin (1981) uses the notation S_ω for the volume flux instead of the mass flux $q=\rho_{air}S_\omega$ used by Lighthill (1978). For a spherical source of radius R_b:

$$S_\omega = 4\pi R_b^2 U \tag{16}$$

where U is the radial velocity. The coefficient 4 is to be suppressed for a circular vent radiating acoustic pressure by ejecting vertical gas at a varying velocity U. By assuming small monochromatic oscillations at frequency ω, acoustic power Π_m radiated in an infinite space is:

$$\Pi_m = \frac{\rho_{air}\omega^2 S_\omega^2}{4\pi c} \tag{17}$$

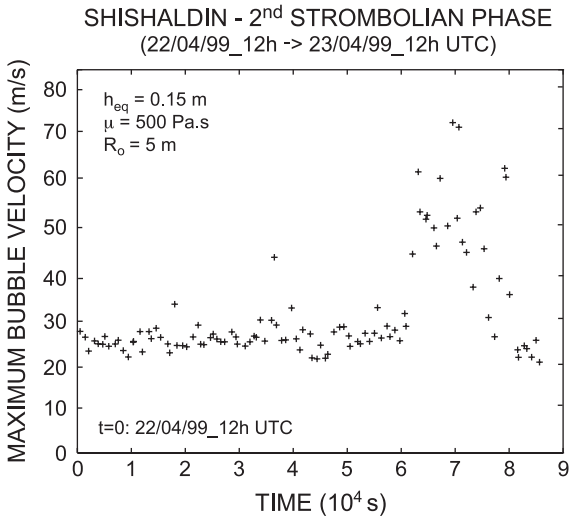

Fig. 16. Maximum magma velocity (m/s) for each largest bubble per 800 s during the second Strombolian phase and estimated from modelling the bubble vibration. Bubble radius R_0 is 5 m, magma thickness above bubble h_{eq} is 0.15 m and magma viscosity μ is 500 Pas. Time $t=0$ is 12:00 h on 22/04/1999 (UTC).

where ρ_{air} is the air density and c the sound speed in air (Temkin, 1981). The radiation of half a bubble in half a space is equivalent to that of a spherical bubble in infinite space (see Eq. (1)). Therefore, Π_m (see Eq. (17)) corresponds to the acoustic radiation produced by each Strombolian explosion at Shishaldin volcano.

For small monochromatic oscillations at frequency ω, the oscillatory velocity U has the same dimension as ωR_b (Landau and Lifshitz, 1987). Using this approximate value of ω in Eq. (17), acoustic power depends mainly on gas velocity U:

$$\Pi_m = K_m \frac{4\pi R_b^2 \rho_{air} U^4}{c} \tag{18}$$

where K_m is an empirical constant. We have just shown that $K_m = 1$ represents the exact solution for a spherical source and $K_m = 1/16$ is the value to be used for a circular flat orifice (Vergniolle and Caplan-Auerbach, 2004a). Our formulation (Eq. (18)) is equivalent to equations used by Woulff and McGetchin (1976), but adds an exact value for K_m.

Note that in all the above analysis the length scale is assumed to be the bubble radius. In theory, it should be taken as the equilibrium radius R_{eq} (see Eq. (5)). However, in practice, R_{eq} is unknown but can be estimated by the minimum bubble radius R_0, which is on the order of the conduit radius. For small oscillations, the two length scales are the same but for mild or strong oscillations, there is a correcting factor in Eq. (18), which accounts for the amplitude of

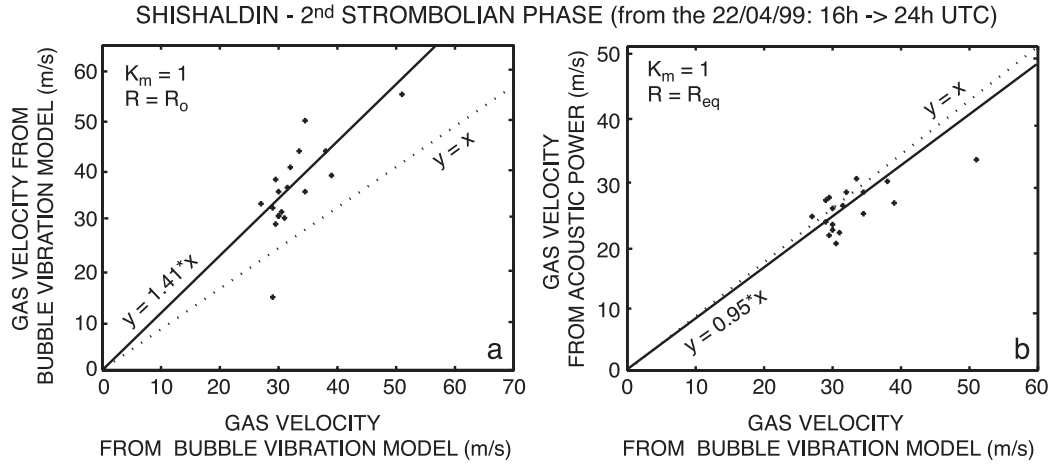

Fig. 17. Comparison between two methods of estimating velocities during the second Strombolian phase (from 16:00 to 24:00 h, the 22nd of April 1999). On x-axis, velocity is calculated by the full modelling of bubble vibration (Eq. (6)). On y-axis, velocity is calculated from acoustic power (Eq. (18)) using (a) the initial bubble radius R_0 and (b) the equilibrium radius R_{eq}.

the oscillation. For simplicity, we estimate gas velocity using the initial bubble radius.

At Shishaldin, gas velocities are calculated from averaging acoustic power over 1.5 s and using a constant K_m of 1 (Eq. (18)). Gas velocities estimated from acoustic power are slightly larger (between 30 and 70 m/s) than values estimated by the full model of bubble vibration (between 30 and 50 m/s) (Fig. 17). The relationship between both estimates is roughly linear with a slope of 1.4 (Fig. 17a). The spreading of the correlation is related to the degree of non-linearity in bubble oscillation, which is always mild. Estimates of velocity from the exact solution of motion during bubble vibration or from acoustic power are exactly the same if using the equilibrium radius (Fig. 17b). Note that velocities have only been estimated for bubble vibration. This calculation ignores possible accelerations effects due to the motion of hot magmatic gas once the bubble has burst. At Stromboli, velocities obtained from modelling of bubble vibration are also smaller than independent estimates of gas velocity above the vent (Weill et al., 1992; Vergniolle and Brandeis, 1996). Therefore, although the acoustic power method overestimates velocities during bubble vibration if using the initial bubble radius, gas velocity, once the bubble has burst, is probably safely estimated by using acoustic power with a constant K_m of 1.

8. Comparison with other volcanoes and conclusion

The occurrence, at Shishaldin, of bubbles whose length is significantly longer than the radius is similar to Stromboli, whose bubbles have lengths between 1 and 25 m for a bubble radius of 1 m (Vergniolle and Brandeis, 1996), and to Etna volcano, with bubble length between 5 and 40 m for a bubble radius of 5 m (Vergniolle, 2003). This is the trademark of a well-developed slug flow (Wallis, 1969). Therefore, bubbles present during the two Strombolian phases of Shishaldin are not long enough to represent an inner gas jet, such as that produced during fire fountains. Because no confirmed fire fountaining episodes were observed at Shishaldin, we feel that this estimate is robust.

Pressure could be used as a very good variable to estimate the "strength" of an eruption. Although very few measurements exist, there is a trend between large overpressure and explosivity. Bubble overpressures have been estimated at ≈ 0.10 MPa at Stromboli (Vergniolle and Brandeis, 1996) and between 0.05 MPa and 0.6 MPa at Etna (Vergniolle, 2003). Although bubble overpressure at Shishaldin can be very strong, our estimates are still on the same order of magnitude as other strong Strombolian eruptions, such as one recorded at Sakurajima volcano (Japan), 0.2–5 MPa (Morrissey and Chouet, 1997). Furthermore, bubble overpressure at Shishaldin is always much smaller than estimates from explosive eruptions, such as Mount Tokachi (Japan) in 1988 (between 0.1 and 1 MPa), Mount Ruapehu (New Zealand, between 0.2 and 5 MPa), the 1975 Ngauruhoe eruption (New Zealand, between 5 and 6 MPa), and Mount Pinatubo (Philippines) in 1991 (≥ 5 MPa) (Morrissey and Chouet, 1997). The initial overpressure at the start of the Mount Saint Helens eruption has been estimated at 7.5 MPa (Kieffer, 1981). The strong overpressure associated with the second Strombolian phase may explain the large amplitude of tremor observed at the time (Thompson et al., 2002).

We next compare gas volume at Shishaldin to other basaltic eruptions. At Shishaldin, the gas volume ejected per bubble, $\approx 1.3 \times 10^4$ and $\approx 1.0 \times 10^4$ m^3 for the first and second Strombolian phases respectively, is larger than that observed at Stromboli, between 2 and 200 m^3 when measured using acoustic data (Vergniolle and Brandeis, 1996) and between 40 and 180 m^3 for one second from COSPEC measurements (Allard et al., 1994). Allard et al. (1994) further note that most degassing at Stromboli occurs passively, rather than during explosions, and this may also be true for Shishaldin, as a gas plume is a constant presence at the summit. At Shishaldin, gas flux ejected at atmospheric pressure, probably mainly CO_2, H_2O and SO_2, is $\approx 3.0 \times 10^3$ m^3/s for the two Strombolian phases. COSPEC measurements, over the main summit craters area at Etna volcano, shows that the gas flux of SO_2 is 22, 2.2×10^3 and 4.4×10^3 m^3/s for the main three kinds of activity at Etna volcano, namely low passive fuming, high Strombolian activity and lava fountains paroxysm (Allard, 1997). Gas volumes expelled per bubble at Shishaldin volcano is also larger than what is estimated from acoustic measurements at Etna volcano, $4.7 \times 10^3 \pm 1.7 \times 10^3$ m^3 (Vergniolle, 2003). The total gas volume ejected per eruptive episode during the

2001 eruption of Etna volcano is $\approx 6.2 \times 10^6$ m^3 for a duration of 4 h, much less than at Shishaldin volcano, 3.3×10^7 m^3 for the first Strombolian phase and 1.0×10^8 m^3 for the second one. Fire fountains at Kilauea volcano correspond to a gas volume at atmospheric pressure between 5.0×10^8 and 3.0×10^9 m^3 for the Pu'u O'o eruption (Vergniolle and Jaupart, 1990), which is more than 20 times that of Shishaldin. Therefore, the large difference in gas volumes is representative of two different eruption dynamics, such as an inner gas jet feeding a fire fountain at a volcano such as Kilauea or a continuous series of large bubbles like at Shishaldin volcano.

Although Shishaldin volcano is difficult to access, acoustic data have proved to be very valuable in quantifying its eruption dynamics. Bubble lengths and overpressure at the surface can be estimated from synthetic waveforms, as well as gas velocity during each Strombolian explosion. Acoustic pressure, which can be easily measured close to an active volcano, allows us to estimate physical variables, such as pressure and velocity needed for understanding the eruptive behaviour.

Acknowledgements

We thank Milton Garcès for taking the initiative to install a pressure sensor at Shishaldin. We are grateful for the support of the Alaska Volcano Observatory, as well as the insights of our colleagues, notably P. Stelling and S.R. McNutt. We thank Dan Osborne, Jay Helmericks, Steve Estes, Tanja Petersen and Guy Tytgat of the Geophysical Institute, UAF for help in retrieving and attempting to calibrate the pressure sensor. We also thank Matthias Hort and two anonymous reviewers whose comments greatly improved the quality of this manuscript. This work was supported by CNRS-INSU (ACI and PNRN: contribution number 323) and by the French Ministère de l'Environnement (number 122/2000). This is a IPGP contribution number 1945.

References

Allard, P., 1997. Endogeneous magma degassing and storage at Mount Etna. Geophys. Res. Lett. 24, 2219–2222.

Allard, P., Carbonelle, J., Metrich, N., Loyer, H., 1994. Sulphur output and magma degassing budget of Stromboli volcano. Nature 368, 326–330.

Batchelor, G.K., 1967. An Introduction To Fluid Dynamics. Cambridge Univ. Press, Cambridge, 615 pp.

Beget, J., Nye, C., Stelling, P., 1998. Postglacial collapse and regrowth of Shishaldin volcano, Alaska, based on historic and prehistoric tephrochronology. Eos Trans. AGU 79, F979.

Blackburn, E.A., Wilson, L., Sparks, R.S.J., 1976. Mechanics and dynamics of Strombolian activity. J. Geol. Soc. (London) 132, 429–440.

Buckingham, M.J., Garcès, M.A., 1996. A canonical model of volcano acoustics. J. Geophys. Res. 101, 8129–8151.

Calvari, S., Coltelli, M., Muller, W., Pompillio, M., Scribano, V., 1994. Eruptive history of the South-Eastern Crater of Mount Etna, from 1971 to 1994. Acta Vulcanol. 5, 11–14.

Caplan-Auerbach, J., McNutt, S.R., 2003. New insights into the 1999 eruption of Shishaldin volcano based on acoustic data. Bull. Volcanol. 65, 405–417.

Chouet, B., Hamisevicz, N., McGetchin, T.R., 1974. Photoballistics of volcanic jet activity at Stromboli, Italy. J. Geophys. Res. 79, 4961–4975.

Chouet, B., Dawson, P., Ohminato, T., Martini, M., Saccorotti, G., Giudicepietro, F., De Luca, G., Milana, G., Scarpa, R., 2003. Source mechanisms of explosions at Stromboli volcano, Italy, determined from moment-tensor inversions of very-long-period data. J. Geophys. Res. 108 (B1), 2019;

Chouet, B., Dawson, P., Ohminato, T., Martini, M., Saccorotti, G., Giudicepietro, F., De Luca, G., Milana, G., Scarpa, R., 2003. Source mechanisms of explosions at Stromboli volcano, Italy, determined from moment-tensor inversions of very-long-period data. ESE 7, 1–25.

Cole, R.H., 1948. Underwater explosions. Princeton Univ. Press, Princeton, USA, 432 pp.

Coltelli, M., Pompilio, M., Del Carlo, P., Calvari, S., Pannucci, S., Scribano, V., 1998. Etna: 1. Eruptive activity, ACVU, 26, 10, 1, 141-148.

Dehn, J., Dean, K.G., Engle, K., Izbekov, P., 2002. Thermal precursors in satellite images of the 1999 eruption of Shishaldin volcano. Bull. Volcanol. 64, 525–534.

Dingwell, D.B., 1998. Recent experimental progress in the physical description of silicic magma relevant to explosive volcanism. In: Gilbert, J.S., Sparks, R.S.J. (Eds.), The physics of explosive volcanic eruptions. Spec. Publ.-Geol. Soc., vol. 145, pp. 9–26.

Dubosclard, G., Cordesses, R., Allard, P., Hervier, C., Coltelli, M., Kornprobst, J., 1999. First testing of a volcano Dopler radar (Voldorad) at Mount Etna, Italy. Geophys. Res. Lett. 26, 3389–3392.

Dubosclard, G., Donnadieu, F., Allard, P., Cordesses, R., Hervier, C., Coltelli, M., Privitera, E., Kornprobst, J., 2004. Dopler radar sounding of volcanic eruption dynamics at Mount Etna. Bull. Volcanol. in press, doi:10.1007/s 00445-003-0324-8.

Fabre, J., Linné, A., 1992. Modelling of two-phase slug flow. Annu. Rev. Fluid Mech. 24, 21–46.

Fournelle, J., 1988. The geology and petrology of Shishaldin vol-

cano, Unimak Island, Aleutian Arc, Alaska. PhD Dissertation thesis, Johns Hopkins University, 507 pp.

Garcès, M.A., McNutt, S.R., 1997. Theory of the airborne sound field generated in a resonant magma conduit. J. Volcanol. Geotherm. Res. 78, 155–178.

Garcès, M.A., Hansen, R.A., Lindquist, K.G., 1998a. Traveltimes for infrasonic waves propagating in a stratified atmosphere. Geophys. J. Int. 135, 255–263.

Garcès, M.A., Hagerty, M.T., Schwartz, S.Y., 1998b. Magma acoustics and time-varying melt properties at Arenal volcano, Costa Rica. Geophys. Res. Lett. 25 (13), 2293–2296.

Garcès, M.A., McNutt, S.R., Hansen, R.A., Eichelberger, J.C., 2000. Application of wave-theoretical seismoacoustic models to the interpretation of explosion and eruption tremor signals radiated by Pavlof volcano, Alaska. J. Geophys. Res. 105 (B2), 3039–3058.

Garcès, M.A., Iguchi, M., Ishihara, K., Morrissey, M., Sudo, Y., Tsutsui, T., 2001. Infrasonic precursors to a Vulcanian eruption at Sakurajima volcano, Japan. Geophys. Res. Lett. 26 (16), 1071–1074.

Hagerty, M.T., Schwartz, S.Y., Garcès, M.A., Protti, M., 2000. Analysis of seismic and acoustic observations at Arenal volcano, Costa Rica, 1995–1997. J. Volcanol. Geotherm. Res. 101, 27–65.

Hort, M., Seyfried, R., 1998. Volcanic eruption velocities measured with a micro radar. Geophys. Res. Lett. 25 (1), 113–116.

Jaupart, C., Vergniolle, S., 1988. Laboratory models of Hawaiian and Strombolian eruptions. Nature 331 (6151), 58–60.

Jaupart, C., Vergniolle, S., 1989. The generation and collapse of a foam layer at the roof of a basaltic magma chamber. J. Fluid Mech. 203, 347–380.

Johnson, J.B., Lees, J.M., 2000. Plugs and chugs: seismic and acoustic observations of degassing explosions at Karymsky, Russia and Sangay, Ecuador. J. Volcanol. Geotherm. Res. 101, 67–82.

Johnson, J.B., Lees, J.M., Gordeev, E.I., 1998. Degassing explosions at Karymsky volcano, Kamchatka. Geophys. Res. Lett. 25, 3999–4002.

Kieffer, S.W., 1981. Fluid dynamics of the May 18 blast at Mount St. Helens. U.S. Geol. Surv. Prof. Pap. 1250, 379.

Kirpatrick, R.D., Lockett, M.J., 1974. The influence of the approach velocity on bubble coalescence. Chem. Eng. Sci. 29, 2363–2373.

Landau, L.D., Lifshitz, E.M., 1986. Course in Theoretical Physics: Theory of Elasticity, vol. 7. Pergamon Press, Oxford, 187 pp.

Landau, L.D., Lifshitz, E.M., 1987. Course in Theoretical Physics: Fluids Mechanics, vol. 6. Pergamon Press, Oxford, 536 pp.

Le Guern, F., Tazieff, H., Vavasseur, C., Zettwoog, P., 1982. Resonance in gas discharge of the Bocca Nuova, Etna (Italy, 1968–1969). J. Volcanol. Geotherm. Res. 12, 161–166.

Leighton, T.G., 1994. The Acoustic Bubble. Academic press, London. 613 pp.

Lighthill, J., 1978. Waves in Fluids. Cambridge Univ. Press, Cambridge. 504 pp.

McGetchin, T.R., Settle, M., Chouet, B.A., 1974. Cinder cone growth modeled after northeast crater, Mount Etna, Sicily. J. Geophys. Res. 79 (23), 3257–3272.

Morrissey, M.M., Chouet, B., 1997. Burst conditions of explosive volcanic eruptions recorded on microbarographs. Science 275, 1290–1293.

Nye, C.J., Keith, T., Eichelberger, J.C., Miller, T.P., McNutt, S.R., Moran, S.C., Schneider, D.J., Dehn, J., Schaefer, J.R., 2002. The 1999 eruption of Shishaldin volcano, Alaska: monitoring a distant eruption. Bull. Volcanol. 64, 507–519.

Plesset, M.S., Mitchell, T.P., 1956. On the stability of the spherical shape of a vapor cavity in liquid. Q. Appl. Math. 13, 419–430.

Plesset, M.S., Prosperetti, A., 1977. Bubble dynamics and cavitation. Annu. Rev. Fluid Mech. 9, 145–185.

Prosperetti, A., 1986. Bubble dynamics. Proc. Int. Sch. Phys. "Enrico Fermi" XCIII, 145–188.

Proussevitch, A.A., Kutolin, V.A., 1986. Surface tension of magmatic melts. Geol. Geophys. 9, 58–67 (in Russian).

Proussevitch, A.A., Sahagian, D.L., 1996. Dynamics of coupled diffusive and decompressive bubble growth in magmatic systems. J. Geophys. Res. 101 (B8), 17447–17455.

Richards, A.F., 1963. Volcanic sounds, investigation and analysis. J. Geophys. Res. 68, 919–928.

Richter, D.H., Eaton, J.P., Murata, K.J., Ault, W.U., Krivoy, H.L., 1970. Chronological narrative of the 1959–60 eruption of Kilauea volcano, Hawaii. U.S. Geol. Surv. Prof. Pap. 537, 1–70.

Ripepe, M., Rossi, M., Saccarotti, G., 1993. Image processing of explosive activity at Stromboli. J. Volcanol. Geotherm. Res. 54, 335–351.

Self, S., Sparks, R.S.J., Booth, B., Walker, G.P.L., 1974. The 1973 Heimaey Strombolian scoria deposit, Iceland. Geol. Mag. 111 (6), 539–548.

Sparks, R.S.J., Bursik, M.I., Carey, S.N., Gilbert, J.S., Glaze, L.S., Sigurdsson, H., Woods, A.W., 1997. Volcanic Plumes. Wiley, Chichester, UK, 574 pp.

Stelling, P., Beget, J., Nye, C., Gardner, J., Devine, J.D., George, R.M.M., 2002. Geology and petrology of ejecta from the 1999 eruption of Shishaldin volcano, Alaska. Bull. Volcanol. 64, 548–561.

Temkin, S., 1981. Elements of Acoustics. Wiley, Chichester, UK, 515 pp.

Thompson, G., McNutt, S.R., Tytgat, G., 2002. Three distinct regimes of volcanic tremor associated with the eruption of Shishaldin volcano, Alaska, April 1999. Bull. Volcanol. 64, 535–547.

Uhira, K., Takeo, M., 1994. The source of explosive eruptions of Sakurajima volcano, Japan. J. Geophys. Res. 99 (B9), 17775–17789.

Vergniolle, S., 1998. Modelling two-phase flow in a volcano. Proc. of 13th Australasian Fluid Mech. Conf., Aristoc offset Printers for Monash University, Melbourne, pp. 647–650. Melbourne.

Vergniolle, S., 2001. Listening to Stromboli volcano as a tool into its volcanic conduit. Eos Trans. AGU 82 (47), F1399.

Vergniolle, S., 2003. Listening to volcanoes as a tool to understand eruption dynamics: Etna (Italy), Shishaldin (Alaska). IUGG Proc., pp. 131–138. Sapporo, Japan.

Vergniolle, S., Brandeis, G., 1994. Origin of the sound generated by Strombolian explosions. Geophys. Res. Lett. 21, 1959–1962.

Vergniolle, S., Brandeis, G., 1996. Strombolian explosions: a large bubble breaking at the surface of a lava column as a source of sound. J. Geophys. Res. 101 (B9), 20433–20448.

Vergniolle, S., Caplan-Auerbach, J., 2004a. Acoustic measurements of the 1999 basaltic eruption of Shishaldin volcano, Alaska: 2) Precursor to the Subplinian activity. J. Volcanol. Geotherm. Res. 137, 153–169. doi:10.1016/j.volgeores. 2004.05.004.

Vergniolle, S., Caplan-Auerbach, J., 2004b. Basaltic and Subplinian plumes: constraints from acoustic measurements at Shishaldin volcano, Alaska. Earth Planet Sci. Lett., Subm.

Vergniolle, S., Caplan-Auerbach, J., 2004c. Acoustic measurements of a Subplinian basaltic eruption: Shishaldin volcano, Alaska, 1999. J. Geophys. Res. Subm.

Vergniolle, S., Caplan-Auerbach, J., 2004d. Chronicle of an explosive basaltic eruption from the sound produced by the 1999 Shishaldin eruption, Alaska. J. Geophys. Res., Subm.

Vergniolle, S., Jaupart, C., 1986. Separated two-phase flow and basaltic eruptions. J. Geophys. Res. 91 (B12), 12842–12860.

Vergniolle, S., Jaupart, C., 1990. The dynamics of degassing at Kilauea volcano, Hawaii. J. Geophys. Res. 95 (B3), 2793–2809.

Vergniolle, S., Brandeis, G., Mareschal, J.C., 1996. Strombolian explosions: eruption dynamics determined from acoustic measurements. J. Geophys. Res. 101 (B9), 20449–20466.

Wallis, G.B., 1969. One Dimensional Two-Phase Flows. Mc Graw Hill, 408 pp.

Weill, A., Brandeis, G., Vergniolle, S., Baudin, F., Bilbille, J., Fevre, J.-F., Piron, B., Hill, X., 1992. Acoustic sounder measurements of the vertical velocity of volcanic jets at Stromboli volcano. Geophys. Res. Lett. 19, 2357–2360.

Wilson, L., 1980. Relationships between pressure, volatile content and ejecta velocity. J. Volcanol. Geotherm. Res. 8, 297–313.

Wilson, L., Head, J.W., 1981. Ascent and eruption of basaltic magma on the earth and moon. J. Geophys. Res. 86, 2971–3001.

Wohletz, K., 2001. Kware Magma v. 2.44.0079, 2001.

Wolfe, E.W., Garcia, M.O., Jackson, D.B., Koyanagi, R.Y., Neal, C.A., Okamura, A.T., 1987. The Puu O'o eruption of Kilauea volcano, episodes 1–20, January 3, 1983 to June 8, 1984. U.S. Geol. Surv. Prof. Pap. 1350, 471–508.

Woulff, G., McGetchin, T.R., 1976. Acoustic noise from volcanoes: Theory and experiments. Geophys. J. R. Astron. Soc. 45, 601–616.